J. Mech. Phys. Solids 158 (2022) 104621

Contents lists available at ScienceDirect

Journal of the Mechanics and Physics of Solids

journal homepage: www.elsevier.com/locate/jmps

Theory of soft solid electrolytes: Overall properties of composite electrolytes, effect of deformation and microstructural design for enhanced ionic conductivity

Kosar Mozaffari [a], Liping Liu [b,*], Pradeep Sharma [a,c,*]

[a] Department of Mechanical Engineering, University of Houston, Houston, TX 77204, USA
[b] Department of Mathematics and Mechanical and Aerospace Engineering, Rutgers University, NJ 08854, USA
[c] Department of Physics, University of Houston, Houston, TX 77204, USA

ARTICLE INFO

Keywords:
Ionic conductivity
Solid composite electrolyte
Heterogeneous media
Electro-diffusive-elastic coupling
Stretchable devices
Li-ion battery
Optimal design

ABSTRACT

Re-chargeable batteries are an important element in the solution to the future of portable energy storage. In that context, electrolytes play a critical role in the adjudication of a battery's capacity, efficiency and operation. In most current embodiments of rechargeable batteries, including the widely researched lithium-ion system, electrolytes are *liquid*. That said, the use of *solid* electrolytes in lieu of their liquid counterparts is being increasingly explored. Solid electrolytes offer increased stability and improved safety and (specifically polymers) are also ideal candidates in the context of stretchable and flexible electronics. Unfortunately, most solid polymer electrolytes possess ionic conductivity that is orders of magnitude lower than typical liquid electrolytes. In this work, we explore the possibility of microstructure design to enhance the effective ionic conductivity of composite polymer electrolytes. We develop a theoretical framework, grounded in thermodynamics and principles of continuum mechanics, to model the coupled deformation, electrostatics and diffusion in heterogeneous electrolytes. Guided by numerical thought experiments, we establish a homogenization procedure that significantly reduces the complexity of the original non-linear problem and derive general analytical expressions for the effective behavior of electrolytes and closed-form solutions for specific microstructures. Using insights from our model, in addition to proposing suggestions for improving the ionic conductivity of solid electrolytes, we are also able to explain several perplexing experimental observations and address questions such as: (i) Why do some experiments show a dramatic *improvement* in the ionic conductivity of nanoparticle-impregnated polymers while others yield a *decrease*? (ii) What is the effect of deformation on ionic conductivity?

1. Introduction

Rechargeable batteries, whether for consumer and portable electronics, green vehicles or simply for our electrical grid, are expected to be an integral part of the future of sustainable clean energy (Chu and Majumdar, 2012; Zito and Ardebili, 2019). The current generation of available battery systems, at least those that are commercially viable or in advanced stages of laboratory development, still fall woefully short of the future demands in terms of the trade-offs between energy density capacity, reliability, efficiency and cost (Tarascon and Armand, 2001; Kasavajjula et al., 2007). Accordingly, intense research in the broadly defined field

---

* Corresponding authors.
E-mail addresses: liu.liping@rutgers.edu (L. Liu), psharma@central.uh.edu (P. Sharma).

https://doi.org/10.1016/j.jmps.2021.104621
Received 21 June 2021; Received in revised form 4 August 2021; Accepted 20 August 2021

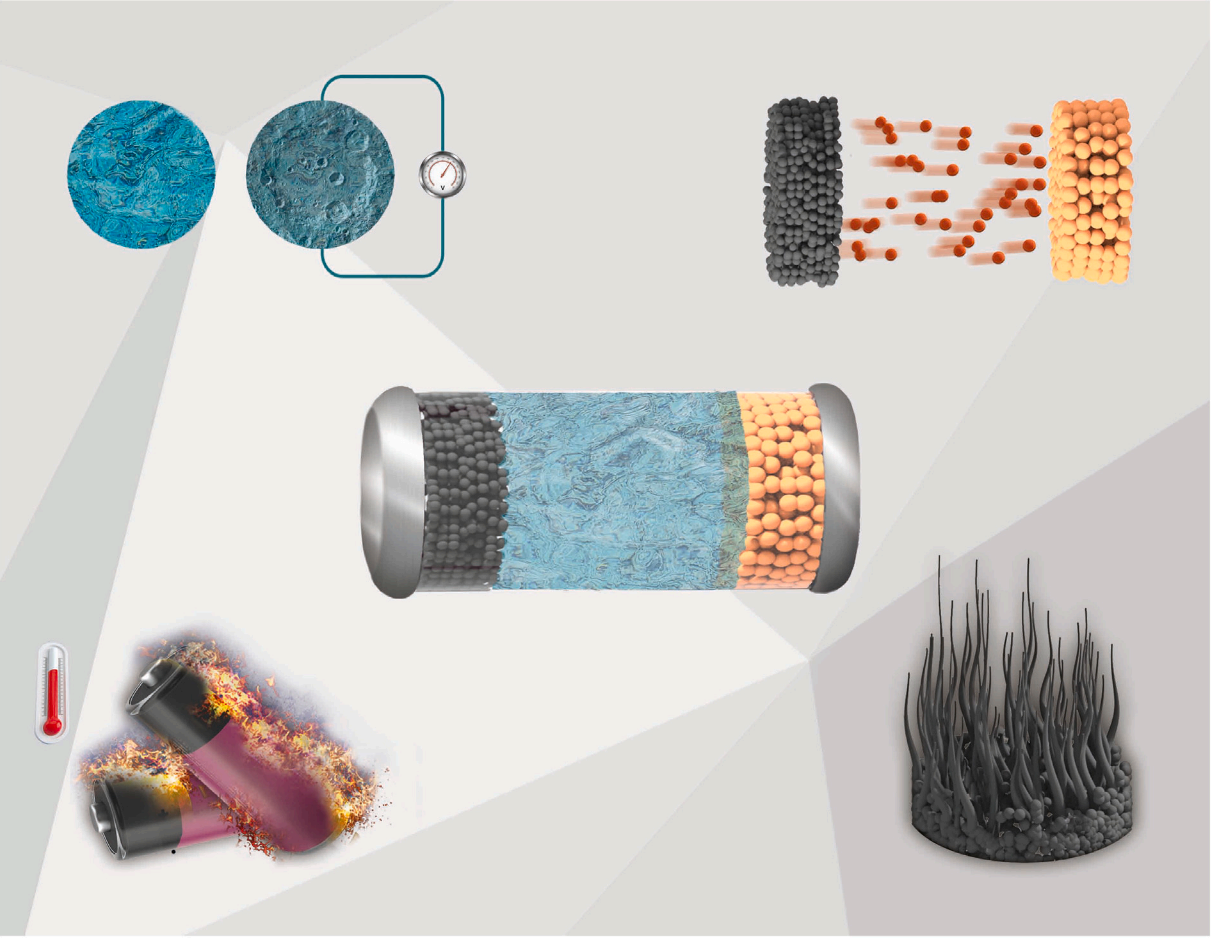

Fig. 1. Schematic of essential characteristics of a typical electrolyte including: electrochemical stability (top left), ionic conductivity (top right), thermal stability (bottom left), suppression of dendrite growth (bottom right).

of materials science is ongoing to develop next-generation batteries. We refer the reader to several expert reviews on this subject that have appeared recently (Goodenough and Park, 2013; Winter and Besenhard, 1999; Lukatskaya et al., 2016).

The energy capacity of a battery, which is amalgamation of its energy density and cyclability,[1] depends primarily on the design and chemistry of the electrodes (Li et al., 2016). It is therefore hardly surprising that a significant effort has been expended on the development of electrode materials (Li et al., 2019; Roy and Srivastava, 2015; Chan et al., 2008; Bower et al., 2011) like Silicon for the Li-ion system (due to its high specific charge density), alternatives to Li-based systems like Sodium (Manthiram and Yu, 2015; Vaalma et al., 2018) and Magnesium (Aurbach et al., 2000), and alternative chemistries (e.g. metal–air battery systems (Jung et al., 2012; Bruce et al., 2012) and Lithium-Sulfur batteries (Manthiram et al., 2014)). In particular, theoretical and computational materials and mechanics community have largely, with some notable exceptions which we will highlight in due course, focused on the understanding and development of electrode materials[2] (Winter and Besenhard, 1999; Kasavajjula et al., 2007; Lukatskaya et al., 2016; Bower et al., 2011; Di Leo et al., 2014; Zhao et al., 2010, 2011; Sethuraman et al., 2010; Chon et al., 2011; Gao and Hong, 2016; Zhang et al., 2015; Lang et al., 2016; Song et al., 2010; Lang et al., 2016; Shen et al., 2020; Chang et al., 2018; Guo et al., 2020; Yan et al., 2017; Cho et al., 2020; Guo et al., 2018; Darbaniyan et al., 2020; Lee et al., 2015; Yan et al., 2015; Xiao et al., 2015).

Electrolytes, as the primary mediator of ion transport between the electrodes, dictate the current density of the battery, temporal stability and safety (Li et al., 2016; Quartarone and Mustarelli, 2011). Notably, the study into both the basic science as well as design of next-generation electrolytes has acquired significant prominence during the past several years (c.f. Zhang et al. (2020c), Fan et al.

---

[1] A measure of repeated charge–discharge cycles before the battery's capacity declines appreciably.

[2] As an example of a well-studied mechanics issue, Silicon anode in a Li-ion battery system can sustain volumetric expansion of close to 300% during a charge–discharge cycle, leading to a heterogeneous stress state, nucleation of defects and micro-cracks and eventual loss of capacity over a short number of cycles.

(2018), Stephan (2006), Balaish et al. (2014), Zhao et al. (2020), Ito and Nohira (2000), Quartarone and Mustarelli (2020)). On that note, as shown schematically in Fig. 1, there are several attributes of an electrolyte that collectively characterize its effectiveness in a battery system e.g. ionic conductivity, electrochemical stability in the voltage range of operation, thermal stability among others.[3]

Research into electrolytes in batteries[4] has, until recently, predominantly focused on liquid electrolytes—the most commonly used in current systems. There are however compelling reasons to understand and develop solid electrolytes. Liquid electrolytes have well-noted safety concerns,[5] and can suffer from poor thermal and electrochemical instability (Quartarone and Mustarelli, 2011). Notably, solid electrolytes are also envisaged to pave the way for the development of novel battery chemistries and offer advantages in terms of safety and inhibiting dendritic growth at metal electrodes (Li et al., 2016; Yang et al., 2017). Finally, we remark that the growing interest in stretchable and flexible electronics requires the concomitant development of stretchable and flexible batteries[6] with solid-state electrolytes . Specifically, from a mechanical viewpoint, in the context of stretchable and flexible electronics and batteries, the electrolyte must be both solid-state as well as soft[7](Tan et al., 2018; Zhang et al., 2015; Xu et al., 2013; Ardebili, 2020; Tang et al., 2012; Li et al., 2013). The larger deformability of soft solid electrolytes can also help with accommodation of the swelling induced strain (and consequent stresses) in electrodes—which is a major issue in the context of Silicon electrode in a Lithium-ion battery system (Manthiram et al., 2017).

Ionic conductivity is arguably the most important, and perhaps the defining, characteristic of an electrolyte. A quick circuit analysis (c.f. Section 3.2) shows that the conversion efficiency from chemical energy of active electrode materials to useful work of the external circuit is given by $R/(R+R_b)$, where R and R_b stand for the resistance of the external circuit and electrolyte respectively. Noting that R_b is inversely proportional to the ionic conductivity of the electrolyte, enhanced ionic conductivity acts to reduce waste heat and temperature and improves the conversion efficiency and overall safety and reliability of the battery. In this sense, liquid electrolytes[8] offer significant advantage over their solid counterparts. Their ionic conductivity is several orders of magnitude larger than those of solid electrolytes.[9] A key challenge in the development of solid electrolytes therefore involves increasing of ionic conductivity.[10] This is particularly exacerbated in applications that require organic solid electrolytes (polymer-based) and have a requirement for large deformation (e.g. stretchable electronics).

Several attempts have been made to increase ionic conductivity of solid polymer-based electrolytes. A partial list of such efforts for the prevention of crystallization includes[11]: (1) addition of plasticizers (Watanabe et al., 1981),[12] (2) making composites in the sense of embedding conductive and non-conductive ceramic particles (Zhang et al., 2020b; Johan et al., 2011; Liu et al., 2015; Wang et al., 2006; Li et al., 2013; Li and Ardebili, 2014), and (3) application of mechanical deformation (Golodnitsky and Peled, 2000; Golodnitsky et al., 2003; Kelly et al., 2016; Minami, 2006). In relation to these attempts, the experimental literature appears to exhibit perplexing trends. While some papers have shown a dramatic improvement – several orders of magnitude increase – in the ionic conductivity by incorporating ceramic inclusions, others have obtained a decrease. For instance, Weston and Steele (Weston and Steele, 1982) observed *no effect* on the effective ionic conductivity by addition of Al_2O_3 particles and even an adverse effect at high volume fraction. Furthermore, there appears to be no clear consensus regarding the effect of particle size and shape and the emergent macroscopic ionic conductivity of the composite polymer electrolyte. In regard to shape, recently studies by Liu et al. (2015, 2017) appeared to indicate that nanowire ceramic inclusion have the best effect in enhancement of the ionic conductivity in comparison to spherical particles. Finally, the coupling of mechanical deformation and ionic conductivity is also unclear. In that context, a key advantage of solid (and especially polymer) electrolytes is the prospects of allowing large deformation. Existing work on tuning ionic conductivity through strain is somewhat sparse. The fact that ionic conductivity ought to be impacted by strain is evident from the pioneering work by Larche and Cahn (1982) in the context of effect of stress on the diffusivity in solids. Indeed experiments by Kelly et al. (2016) showed 400% improvement of ionic conductivity in PEO thin films under 15% tensile strain. In the regime of deformation in the experiments by Kelly et al. (2016), a linear relation between ionic conductivity and strain was found. A perspective on pertinent mechanics issues pertaining to ionic conductivity in solid electrolytes may be found in a recent article by Ardebili (2020).

---

[3] In addition, like with electrode materials, there is also significant interest in developing electrolytes that are environmentally friendly and contain abundantly available constituents.

[4] Although we have primarily focused on the role of electrolytes (specifically solid electrolytes) in the context of batteries, we remark that soft solid electrolytes are of significant interest in the burgeoning field of iontronics (Yang and Suo, 2018; Keplinger et al., 2013; Sun et al., 2014).

[5] A heavily publicized battery failure incident involved in Boeing 787 Dreamliner airplanes (Williard et al., 2013). A Lithium-ion liquid electrolyte based battery is quite inflammable and prone to exploding under certain situations.

[6] There is also a need for developing batteries that are of irregular shape which is best accomplished via soft materials.

[7] There are several types of solid electrolytes which include ceramics (Wang et al., 2015; Bachman et al., 2016), polymer gels (Wang et al., 2002) as well as solid polymers (Quartarone and Mustarelli, 2011; Fenton, 1973).

[8] Liquid electrolytes also are able to wet the electrode much more intimately thus mitigating the issue of interfacial charge transfer across electrode–electrolyte.

[9] The ionic conductivity of ceramics and solid polymers are respectively in the order of 10^{-4} S.cm^{-1} and below 10^{-6} S.cm^{-1} at room temperature (MacGlashan et al., 1999; Pitawala et al., 2007); This is while their liquid counterparts have the ionic conductivity above 10^{-3} S.cm^{-1} at room temperature which is the necessary condition for the operation of most of the electronic devices.

[10] As already indicated, there are other attributes of an electrolyte that are important also such as cation transference number (Gray and Gray, 1991) but a discussion of that is beyond the scope of the present article.

[11] A discussion of the atomistic scale conduction mechanism in solid polymers—whether crystalline ceramics, semi-crystalline polymers or amorphous polymers, is beyond the scope for the current article. The reader is referred to the following review article for further information (Zou et al., 2020). Suffice to say that low ionic conductivity of solid polymer electrolytes is attributed to crystallinity.

[12] Plasticizers can enhance ionic conductivity however at the cost of mechanical instability (Stephan, 2006; Watanabe et al., 1981)

Although ionic conductors, in various guises, have been an active topic of research, in recent years there has been a focused interest on the development of theoretical models that describe the confluence of mechanics, diffusion of ions, and electrostatics in electrolytes. In the context of rigid ionic conductors, the ionic transport is well-known to follow the so-called Poisson–Boltzmann–Nernst–Planck equations and are well-studied in the context of semiconductors.[13] In the mechanics literature, the theory of electrolytes has been revisited by numerous groups with varying stylistic choices and emphasis (Xiao and Bhattacharya, 2008; Hong et al., 2010; Wang and Hong, 2011; Rejovitzky et al., 2015; Grazioli et al., 2019; Zhang et al., 2020a; Ganser et al., 2019; Narayan et al., 2021; Marshall and Dayal, 2014) and sometimes with applications other than battery-electrolytes e.g. ferroelectric semiconductors (Xiao and Bhattacharya, 2008), polymer–metal systems for actuation (Narayan et al., 2021) among others. Of course, frequently, the incorporation of deformation has been a key ingredient in the mechanics literature. In terms of electrolyte behavior via microstructural design and homogenization, we highlight the work of via Sillamoni and Idiart (2015) who took a first step in presenting a coarse-graining approach for rigid electrolytes with an inclusion–matrix morphology.

Given the context established in the preceding paragraphs and the key issues and questions that come to the fore, their redressal is the central goal of our paper. Accordingly, in this paper:

- We establish a suitable theory of ionic conduction in soft deformable solid electrolytes, predicated on the principles of thermodynamics and continuum mechanics. We have attempted to keep our theory as general as possible so as to allow facile future modification as well as reduction to special cases such as Biot's theory of poroelasticity and others.
- Using solutions to simple boundary value problems as a guide, we simplify the homogenization problem for composite electrolytes (and the otherwise analytically intractable nonlinear partial differential equations) and provide estimates of effective ionic conductivity. We also establish Hashin–Sthrikman type variational bounds.
- In light of our theory and homogenization results, we attempt to answer the following question: Why do some experiments show a dramatic improvement in the ionic conductivity of particle-impregnated polymers while others yield a decrease?
- Ionic conductivity of composite electrolytes appears to be size-dependent and contradictory results exist in the literature. How does our theory reconcile the experimental observations?
- We determine the role of deformation on the emergent ionic conductivity of a solid composite electrolyte.

The outline of the paper is as follows: In Section 2, we present a nonlinear continuum theory for electro-elastic-diffusive solids and derive relevant constitutive equations. In Section 3, we probe the central idea underpinning the homogenization procedure for the defined boundary value problem through some simple examples. Based on these, we propose simplified steps for the homogenization of multiphase electrolytes, and furthermore, establish Hashin–Shtrikman type variational bounds. In Section 4, we discuss examples of special (solvable) microstructures including 1D multiphase electrolyte, circular fiber inclusions, and spherical inclusions by the procedure introduced in Section 3. Finally, in Section 5, the obtained homogenized results from Section 4 are compared to the experimental measurements in the literature as well insights from our model to enhance ionic conductivity of electrolytes.

Notation. For brevity, we use direct notation in this paper. Vectors and tensors are shown by bold symbols such as $\mathbf{a}, \mathbf{A}$. The inner product between two vectors $\mathbf{a}, \mathbf{b} \in \mathbb{R}^3$ is defined as $\mathbf{a} \cdot \mathbf{b} = (\mathbf{a})_i (\mathbf{b})_i$ and the tensor product between two vectors $\mathbf{a}, \mathbf{b} \in \mathbb{R}^3$ is defined as $(\mathbf{a} \otimes \mathbf{b})_{ij} = (\mathbf{a})_i (\mathbf{b})_j$. The inner product between matrices $\mathbf{A}$ and $\mathbf{B}$ of the same size is defined as $\mathbf{A} \cdot \mathbf{B} := \mathrm{Tr}(\mathbf{A}^T \mathbf{B}) = (\mathbf{A})_{ij} (\mathbf{B})_{ij}$.

2. A continuum theory for electro-elastic-diffusive systems

In this section, we develop a theoretical framework for electro-elastic-diffusive solids. As already alluded to in the prior section, the central equations, in various forms and derived with different flavors, may be found in the literature (Xiao and Bhattacharya, 2008; Hong et al., 2010; Wang and Hong, 2011; Rejovitzky et al., 2015; Grazioli et al., 2019; Zhang et al., 2020a; Ganser et al., 2019; Narayan et al., 2021; Marshall and Dayal, 2014). We favor a slightly different approach in the derivation and arguably, our handling of the electrostatics distinguishes the derivation from others. We primarily follow the approach by Xiao and Bhattacharya (2008) whose focus was deformable, conducting ferroelectrics and have also used it successfully in a yet another non-equilibrium setting (Darbaniyan et al., 2019). For simplicity, we begin first with an elastic-diffusive system. Later, in Section 2.2 we extend the theory to include electrostatics.

2.1. Elastic-diffusive systems

As illustrated in Fig. 2, we consider a continuum body in which diffusion of ions (or molecules) is coupled with elasticity. We are interested in establishing a continuum model for the elastic-diffusive behaviors of the body that is consistent with the fundamental thermodynamic laws. To this end, we begin with the assumption that the thermodynamic state of the system is described by deformation $\mathbf{y}(\cdot, t) : \Omega_R \to \Omega(t)$ and ion volumetric concentration $c(\cdot, t) : \Omega_R \to \mathbb{R}$ in the reference configuration. As usual, we denote by

$$\mathbf{F} = \nabla \mathbf{y}, \qquad \mathbf{C} = \mathbf{F}^T \mathbf{F}, \qquad J = \det \nabla \mathbf{y}$$

---

[13] We remark here, and this is essentially just our personal opinion, that although well-grounded physically, the usual derivations of the Poisson–Boltzmann–Nernst–Planck equations in physics literature do not follow the systematic postulate-based philosophy of continuum mechanics which we find somewhat unsatisfying.

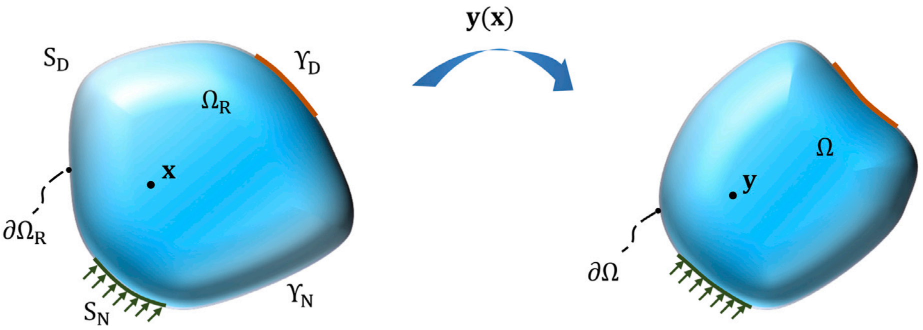

Fig. 2. An elastic-diffusive body subject to external mechanical traction on S_N, prescribed displacement on S_D where $S_D = \partial\Omega_R/S_N$, connected to a solution of ions on Υ_D and prescribed to directional flux perpendicular to the boundary on Υ_N where $\Upsilon_N = \partial\Omega_R/\Upsilon_D$. .

the deformation gradient, Cauchy–Green tensor and deformation Jacobian. The interactions between the body Ω_R and external system are defined by a set of mechanical and chemical boundary conditions. As illustrated in Fig. 2, let S_D and S_N be a subdivision of $\partial\Omega_R$ on which the following mechanical boundary conditions are enforced:

$$\begin{cases} \mathbf{y}(\mathbf{x},t) = \mathbf{y}_b(\mathbf{x},t) & \text{on } S_D, \\ \text{applied external traction} = \mathbf{t}^e(\mathbf{x},t) & \text{on } S_N, \end{cases} \tag{1}$$

where $\mathbf{y}_b(\cdot,t)$ (resp. $\mathbf{t}^e(\cdot,t)$) : S_D(resp. S_N) $\to \mathbb{R}^3$ is the prescribed boundary position (resp. traction). Also, let Υ_D and Υ_N be another subdivision of $\partial\Omega_R$ for prescribing the chemical boundary conditions:

$$\begin{cases} \mu = \mu^e(\mathbf{x},t) & \text{on } \Upsilon_D, \\ \mathbf{J}\cdot\mathbf{n} = J^e & \text{on } \Upsilon_N, \end{cases} \tag{2}$$

where $\mathbf{J}(\cdot,t) : \Omega_R \to \mathbb{R}^3$ (resp. $\mu(\cdot,t) : \Omega_R \to \mathbb{R}$) is the ionic flux (resp. chemical potential), and $\mu^e(\cdot,t) : \Upsilon_D \to \mathbb{R}$ (resp.$J^e(\cdot,t)$) : $\Upsilon_N \to \mathbb{R}$ is the prescribed boundary chemical potential (resp. prescribed directional flux perpendicular to the boundary).[14] Physically, the boundary chemical potential μ^e is dictated by the materials of active electrodes. By the conservation law of ions we have[15]

$$\dot{c} + \mathrm{div}\mathbf{J} = 0 \quad \text{in } \Omega_R. \tag{3}$$

The external system can do work on the body via mechanical tractions or transport of ions across the boundary. The rate of work done on the body Ω_R is given by

$$\dot{W} = \int_{\partial\Omega_R} \dot{\mathbf{y}}\cdot\mathbf{t}^e - \int_{\partial\Omega_R} \mu^e \mathbf{J}\cdot\mathbf{n}. \tag{4}$$

To achieve a closed differential system governing the elastic-diffusion of the body, we need a few hypotheses concerning the *equilibrium* and *non-equilibrium* behavior of the body. Our first hypothesis concerns the behavior of the body Ω_R in *equilibrium states*.

(H1) The free energy of the body *alone* is given by the functional:

$$\begin{aligned} U[\mathbf{y},c] &= U_b[\mathbf{y},c] + U_{\mathrm{elect}}, \\ U_b[\mathbf{y},c] &= \int_{\Omega_R} \Psi(\nabla\mathbf{y},c), \end{aligned} \tag{5}$$

where $\Psi : \mathbb{R}^{3\times3}\times\mathbb{R} \to \mathbb{R}$ is the free energy density and U_{elect} is the electric energy associated with charges and/or polarizations. Since in this section, we will only consider the coupling of elasticity and diffusion, we set $U_{\mathrm{elect}} \equiv 0$. For ionic diffusion in an electron-conductive electrode whose electron-conductivity is much higher than ion-conductivity, the electrode will essentially remain in an electrically equipotential state (as seen by ions) and thus the present setup does apply to the elastic-diffusive coupling of ions in electron-conductive electrodes. The electro-elastic-diffusive coupling will be addressed in Section 2.2 for electrolytes that are ion-conductive but electron-insulating.

We remark that the particular functional form of Ψ defines the constitutive behavior of the body in quasi-static isothermal processes. First of all, by the principles of frame indifference and material symmetries, we have

$$\begin{cases} \Psi(\mathbf{RF},c) = \Psi(\mathbf{F},c) & \forall\, \mathbf{R} \in SO(3), \\ \Psi(\mathbf{FQ},c) = \Psi(\mathbf{F},c) & \forall\, \mathbf{Q} \in \mathcal{G}, \end{cases} \tag{6}$$

---

[14] In what follows, given the physical context of what we are interested in, will shall set $J^e = 0$.

[15] Eq. (3) is standard and follows from the mass balance of diffusing species in the absence of sink and source terms as $\int_{\Omega_R} \dot{c} = -\int_{\partial\Omega_R} \mathbf{J}\cdot\mathbf{n}$ for any subbody. By divergence theorem, this simplifies to $\int_{\Omega_R} [\dot{c} + \mathrm{div}\mathbf{J}] = 0$.

where $SO(3)$ is the set of all rigid rotations and $\mathcal{G} \subset SO(3)$ is the group associated with material symmetries. For simplicity, we assume that the material is isotropic with $\mathcal{G} = SO(3)$. By (5), the rate of change of free energy of the body in all isothermal processes is given by

$$\dot{U}_b = \frac{d}{dt}\int_{\Omega_R} \Psi(\nabla\mathbf{y}, c) = \int_{\Omega_R} [\frac{\partial\Psi(\mathbf{F}, c)}{\partial\mathbf{F}}\Big|_{(\nabla\mathbf{y},c)} \cdot \nabla\dot{\mathbf{y}} + \frac{\partial\Psi(\mathbf{F}, c)}{\partial c}\Big|_{(\nabla\mathbf{y},c)} \dot{c}]. \tag{7}$$

For brevity, we introduce notation:

$$\mathbf{P} := D_{\mathbf{F}}\Psi(\nabla\mathbf{y}, c) = \frac{\partial\Psi(\mathbf{F}, c)}{\partial\mathbf{F}}\Big|_{(\nabla\mathbf{y},c)}, \qquad \mu := D_c\Psi(\nabla\mathbf{y}, c) = \frac{\partial\Psi(\mathbf{F}, c)}{\partial c}\Big|_{(\nabla\mathbf{y},c)}. \tag{8}$$

By substituting (8) into (7) we obtain:

$$\begin{aligned} \dot{U}_b &= \int_{\Omega_R} [\mathbf{P} \cdot \nabla\dot{\mathbf{y}} + \dot{c}\mu] = \int_{\Omega_R} [\mathbf{P} \cdot \nabla\dot{\mathbf{y}} - \mu\nabla \cdot \mathbf{J}] \\ &= \int_{\Omega_R} [-(\mathrm{div}\mathbf{P}) \cdot \dot{\mathbf{y}} + \mathbf{J} \cdot \nabla\mu] + \int_{\partial\Omega_R} [\dot{\mathbf{y}} \cdot (\mathbf{P}\mathbf{n}) - (\mathbf{J} \cdot \mathbf{n})\mu], \end{aligned} \tag{9}$$

where $\mathbf{n}$ is the outward unit normal on $\partial\Omega_R$, the second equality follows from the conservation law (3), and the last equality follows from the divergence theorem. Physically, we recognize $\mathbf{P}$ and μ as the local *internal* Piola–Kirchhoff stress and chemical potential inside the body Ω_R in quasi-static isothermal processes, respectively.

The precise functional form of $\Psi = \Psi(\mathbf{F}, c)$ can in principle be determined by experimental measurements. For example, when the body is subjected to a uniform external traction $\mathbf{t}^e = \mathbf{P}^e\mathbf{n}$ ($\mathbf{P}^e \in \mathbb{R}^{3\times3}$ is constant and $\mathbf{n}$ is the unit outward normal) and allowed to exchange ions with an external reservoir with chemical potential μ^e, we can measure the equilibrium deformation gradient and concentration $(\mathbf{F}_0, c_0)$ of the body which are assumed to be uniform. Then the total free energy of the system can be identified as

$$F[\mathbf{y}, c] = U_b[\mathbf{y}, c] - \mu^e \int_{\Omega_R} c - \int_{\partial\Omega_R} \mathbf{y} \cdot \mathbf{P}^e\mathbf{n}.$$

From the principle of minimum free energy, we infer that the equilibrium deformation gradient and concentration $(\mathbf{F}_0, c_0)$ minimize the above total free energy and hence necessarily satisfy

$$\mathbf{P}^e = \frac{\partial\Psi(\mathbf{F}, c)}{\partial\mathbf{F}}\Big|_{(\mathbf{F}_0,c_0)}, \qquad \mu^e = \frac{\partial\Psi(\mathbf{F}, c)}{\partial c}\Big|_{(\mathbf{F}_0,c_0)}. \tag{10}$$

Then the free energy density function $\Psi = \Psi(\mathbf{F}, c)$ can be obtained by directly integrating the above equations, i.e., from experimentally measured data: $\mathbf{P}^e = \mathbf{P}^e(\mathbf{F}_0, c_0)$ and $\mu^e = \mu^e(\mathbf{F}_0, c_0)$.

From the definition and (4), the rate of energy dissipation $\dot{D} = \dot{W} - \dot{U}$ in isothermal processes is given by

$$\begin{aligned} \dot{D} &= \int_{\Omega_R} [(\mathrm{div}\mathbf{P}) \cdot \dot{\mathbf{y}} - \mathbf{J} \cdot \nabla\mu] \\ &+ \int_{\partial\Omega_R} \dot{\mathbf{y}} \cdot (\mathbf{t}^e - \mathbf{P}\mathbf{n}) - \int_{\Upsilon_D} (\mathbf{J} \cdot \mathbf{n})(\mu^e - \mu). \end{aligned} \tag{11}$$

(H2) By the Second Law of Thermodynamics, the rate of energy dissipation $\dot{D} \geq 0$ for all isothermal processes. To guarantee this, using Coleman–Noll type arguments, we can propose the following.[16]

(i) Non-negative rate of energy dissipation by satisfying

$$-\mathbf{J} \cdot \nabla\mu \geq 0 \quad \text{in } \Omega_R. \tag{12}$$

A choice of a constitutive law which satisfies the aforementioned inequality is proposing a linear relation between the “drift velocity" and “driving force” as follows:

$$\mathbf{v} = -\gamma\nabla\mu \quad \text{i.e.} \quad \mathbf{J} = c\mathbf{v} = -c\gamma\nabla\mu \qquad \text{in } \Omega_R, \tag{13}$$

where $\gamma > 0$ is called the mobility of the ion and assumed to be a material constant and independent ionic concentration c.

(ii) Instantaneous mechanical balance:

$$\mathrm{div}\mathbf{P} = 0 \quad \text{in } \Omega_R. \tag{14}$$

(iii) Boundary conditions:

$$\mu = \mu^e \qquad \text{on } \Upsilon_D, \qquad \mathbf{P}\mathbf{n} - \mathbf{t}^e = 0 \quad \text{on } S_N. \tag{15}$$

From (11) and (13)–(15) we find the rate of energy dissipation is given by

$$\dot{D} = \int_{\Omega_R} c\gamma|\nabla\mu|^2 \geq 0, \tag{16}$$

---

[16] There are alternate ways to guarantee compliance with the Second Law and in addition provide guidance on the form of constitutive law, e.g. the maximum rate of entropy production principle, c.f. Xu et al. (2016).

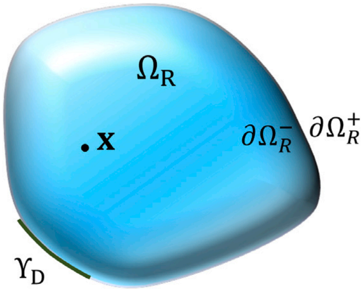

Fig. 3. Schematic of an ionic conductive electrolyte and its boundaries.

which guarantees the satisfaction of the Second Law for the relevant processes.

To summarize, by (1), (2), (3), (8), and (13)–(15) we obtain the boundary value problem for $(\mathbf{y}, c)$ that governs the elastic-diffusive isothermal processes:

$$\begin{cases} \operatorname{div}[D_{\mathbf{F}}\Psi(\nabla\mathbf{y}, c)] = 0 & \text{in } \Omega_R, \\ [D_{\mathbf{F}}\Psi(\nabla\mathbf{y}, c)]\mathbf{n} - \mathbf{t}^e = 0 & \text{on } S_N, \\ \mathbf{y} = \mathbf{y}_b & \text{on } S_D, \end{cases} \tag{17}$$

and

$$\begin{cases} \dot{c} = \operatorname{div}(c\gamma\nabla\mu), \qquad \mu = D_c\Psi(\nabla\mathbf{y}, c) & \text{in } \Omega_R, \\ \mathbf{n}\cdot\nabla\mu = 0 & \text{on } \Upsilon_N, \\ \mu = \mu^e & \text{on } \Upsilon_D. \end{cases} \tag{18}$$

Provided with suitable initial conditions $(\mathbf{y}(\mathbf{x}, t), c(\mathbf{x}, t))|_{t=0} = (\tilde{\mathbf{y}}(\mathbf{x}), \tilde{c}(\mathbf{x}))$, we can solve the above coupled system of differential Eqs. (17)–(18) to determine the evolution of state variables $(\mathbf{y}, c)$.

We remark that the above formulation of elastic-diffusion is versatile since the free energy density function and the dissipation-rate density function admit many possible choices. In the Appendix A, we outline the reduction of the current framework to the classic linear Biot's theory of poroelasticity and the theory of nonlinear swelling of hydrogels.

2.2. Electro-elastic-diffusive systems

We now consider the effect of electric field on the transport of ions in electrolytes (a schematic is illustrated in Fig. 3). Let $\xi : \Omega_R \to \mathbb{R}$ be the electric potential and for simplicity, assume the boundary potential ξ^e on Υ_D is controlled by an external circuit:

$$\xi = \xi^e(\mathbf{x}) \qquad \text{on } \Upsilon_D. \tag{19}$$

The mechanical and chemical boundary conditions remain the same as in Section 2.1 and given by (1) and (2), respectively. Further, denote by q the electric charge associated with each mobile ion and therefore, the electrical current density is given by $\mathbf{J}_e = q\mathbf{J}$. For the electrolyte body Ω_R, analogous to (4), we identify the rate of work done to the body as given by Kovetz (2000)

$$\dot{W} = \int_{\partial\Omega_R^+} \dot{\mathbf{y}}\cdot\mathbf{t}^e - \int_{\partial\Omega_R^+} (\mu^e + q\xi^e)(\mathbf{J}\cdot\mathbf{n}) - \int_{\partial\Omega_R^-} \xi(\dot{\tilde{\mathbf{D}}}\cdot\mathbf{n}), \tag{20}$$

where $\tilde{\mathbf{D}} = -\epsilon(\mathbf{x})J\mathbf{C}^{-1}\nabla\xi$ is the nominal electric displacement, $\partial\Omega_R^+$ (resp. $\partial\Omega_R^-$) means the boundary value at the exterior (resp. interior) of $\partial\Omega$ (as shown in Fig. 3), and $[\![\square]\!] = \square\big|_{\partial\Omega_R^+} - \square\big|_{\partial\Omega_R^+}$ is the jump of $\square$ across the interface. Physically, the first and second terms in (20) arise from the mechanical work and transport of ions across the interface, and the last term arises from the electric work in analogy with charging a capacitor. Here, across an interface the electric potential ξ may be discontinuous because of the presence of chemical potential.

Next, we calculate the rate of change of free energy of the body. It is necessary to include the electrical energy U_{elect} associated with polarization and electric field generated by mobile ions and polarization. Neglecting dynamical effects (i.e., the coupling with time-dependent magnetic fields), the electric field in the reference configuration satisfies the Maxwell equation:

$$\operatorname{div}\tilde{\mathbf{D}} = \operatorname{div}(-\epsilon(\mathbf{x})J\mathbf{C}^{-1}\nabla\xi) = q(c - c_0(\mathbf{x})) \qquad \text{in } \Omega_R, \tag{21}$$

where $\epsilon(\mathbf{x})$ is the electric permittivity, and $c_0 : \Omega_R \to \mathbb{R}$ is the immobile ion concentration that would neutralize the mobile ions in a natural equilibrium state. For simplicity, we assume that the electric permittivity of electrolyte is independent of deformation, i.e.,

$$\mathbf{p} = -(\epsilon - \epsilon_0)\nabla_{\mathbf{y}}\xi \qquad \text{in } \Omega, \tag{22}$$

where ϵ_0 is the vacuum permittivity and $\mathbf{p}$ represents the polarization in the current configuration. Since ions and electrons are mobile and “free”, from discussions by Liu (Liu, 2013) and (22), we identify the bulk electrical energy U_{elect} stored in the system as

$$U_{\text{elect}}[\mathbf{y}, c] = \int_{\Omega} [\frac{\epsilon_0}{2}|\nabla_{\mathbf{y}}\xi|^2 + \frac{|\mathbf{p}|^2}{2(\epsilon(\mathbf{x}) - \epsilon_0)}] = \int_{\Omega_R} \frac{\epsilon(\mathbf{x})}{2} J|\mathbf{F}^{-T}\nabla\xi|^2, \tag{23}$$

where the last equality follows from changing integration variables $\mathbf{y} \to \mathbf{x}$.

To ensure consistency with the Second Law, we need to calculate the rate of energy dissipation of the system. This calculation is a bit technical and gives rise to the so-called Maxwell stress. The final result and implication is however physically intuitive. First, by repeating the calculations in (9)–(11), we find that

$$\dot{U}_b[\mathbf{y}, c] = \int_{\Omega_R} [-(\text{div}\mathbf{P}) \cdot \dot{\mathbf{y}} + \mathbf{J} \cdot \nabla\mu] + \int_{\partial\Omega_R^-} [\dot{\mathbf{y}} \cdot (\mathbf{P}\mathbf{n}) - (\mathbf{J} \cdot \mathbf{n})\mu]. \tag{24}$$

Taking time derivative of (21) we have

$$\nabla \cdot \dot{\tilde{\mathbf{D}}} = \nabla \cdot [-\epsilon(\mathbf{x})\frac{d}{dt}(J\mathbf{C}^{-1}\nabla\xi)] = q\dot{c} \qquad \text{in } \Omega_R. \tag{25}$$

For brevity, denote by Darbaniyan et al. (2019)

$$\dot{\overline{J\mathbf{C}^{-1}}} = \frac{d}{dt}(J\mathbf{C}^{-1}) = -J\mathbf{F}^{-1}\nabla\dot{\mathbf{y}}\mathbf{C}^{-1} - J\mathbf{C}^{-1}(\nabla\dot{\mathbf{y}})\mathbf{F}^{-1} + J(\mathbf{F}^{-T} \cdot \nabla\dot{\mathbf{y}})\mathbf{C}^{-1}. \tag{26}$$

Multiplying (25) by ξ and integrating by parts, we obtain

$$\begin{aligned}\int_{\Omega_R} q\dot{c}\xi &= -\int_{\Omega_R} \xi\nabla \cdot [\epsilon(\mathbf{x})\frac{d}{dt}(J\mathbf{C}^{-1}\nabla\xi)] \\ &= -\int_{\partial\Omega_R^-} \xi[\mathbf{n} \cdot \frac{d}{dt}(\epsilon(\mathbf{x})J\mathbf{C}^{-1}\nabla\xi)] + \int_{\Omega_R} \epsilon(\mathbf{x})\Big[\nabla\xi \cdot \dot{\overline{J\mathbf{C}^{-1}}}\nabla\xi + \nabla\dot{\xi} \cdot (J\mathbf{C}^{-1}\nabla\xi)\Big].\end{aligned} \tag{27}$$

Meanwhile, comparing the continuity equation (3) with (25) or by the Maxwell equation $\mathbf{J}_e + \dot{\tilde{\mathbf{D}}} = \nabla \times \mathbf{H} = 0$, we identify the electric current density

$$\dot{\tilde{\mathbf{D}}} = -\epsilon(\mathbf{x})\frac{d}{dt}(J\mathbf{C}^{-1}\nabla\xi) = -\mathbf{J}_e = -q\mathbf{J} \qquad \text{in } \Omega_R. \tag{28}$$

Therefore, (27) can be rewritten as

$$\int_{\Omega_R} \epsilon(\mathbf{x})\nabla\dot{\xi} \cdot (J\mathbf{C}^{-1}\nabla\xi) = \int_{\Omega_R} \Big[-\epsilon(\mathbf{x})\nabla\xi \cdot \dot{\overline{J\mathbf{C}^{-1}}}\nabla\xi + q\dot{c}\xi\Big] + \int_{\partial\Omega_R^-} q\xi(\mathbf{n} \cdot \mathbf{J}). \tag{29}$$

Further, by (26) we introduce

$$\begin{aligned}&\frac{\epsilon(\mathbf{x})}{2}\nabla\xi \cdot \dot{\overline{J\mathbf{C}^{-1}}}\nabla\xi =: -\nabla\dot{\mathbf{y}} \cdot \boldsymbol{\Sigma}_{\text{MW}}, \\ &\boldsymbol{\Sigma}_{\text{MW}}(\mathbf{x}) = -\frac{\epsilon(\mathbf{x})}{2}J|\mathbf{F}^{-T}\nabla\xi|^2\mathbf{F}^{-T} + \epsilon(\mathbf{x})J(\mathbf{F}^{-T}\nabla\xi) \otimes (\mathbf{F}^{-T}\nabla\xi).\end{aligned} \tag{30}$$

Physically we identify $\boldsymbol{\Sigma}_{\text{MW}}$ as the Piola–Maxwell stress. In summary, by taking time derivative of (23) we find the rate of change of electrical energy U_{elect} as (Xiao and Bhattacharya, 2008):

$$\begin{aligned}\dot{U}_{\text{elect}}[\mathbf{y}, c] &= \int_{\Omega_R} [\frac{\epsilon(\mathbf{x})}{2}\nabla\xi \cdot (\dot{\overline{J\mathbf{C}^{-1}}}\nabla\xi) + \epsilon(\mathbf{x})\nabla\dot{\xi} \cdot (J\mathbf{C}^{-1}\nabla\xi)] \\ &= \int_{\Omega_R} \Big[\nabla\dot{\mathbf{y}} \cdot \boldsymbol{\Sigma}_{\text{MW}} + \dot{c}q\xi\Big] + \int_{\partial\Omega_R^-} q\xi(\mathbf{J} \cdot \mathbf{n}) \\ &= \int_{\Omega_R} \Big[-\dot{\mathbf{y}} \cdot \text{div}\boldsymbol{\Sigma}_{\text{MW}} + \mathbf{J} \cdot \nabla(q\xi)\Big] + \int_{\partial\Omega_R^-} \dot{\mathbf{y}} \cdot (\boldsymbol{\Sigma}_{\text{MW}})\mathbf{n}\end{aligned} \tag{31}$$

where the last equality follows from (29) and (30).

From (20), (24) and (31) we find that the rate of energy dissipation can be written as

$$\begin{aligned}\dot{D} &= \dot{W} - \dot{U}_b - \dot{U}_{\text{elect}} \\ &= \int_{\partial\Omega_R^+} \mathbf{t}^e \cdot \dot{\mathbf{y}} - \int_{\partial\Omega_R^+} (\mathbf{J} \cdot \mathbf{n})(\mu^e + q\xi^e) + \int_{\Omega_R} [\text{div}(\mathbf{P} + \boldsymbol{\Sigma}_{\text{MW}}) \cdot \dot{\mathbf{y}} - \mathbf{J} \cdot \nabla(\mu + q\xi)] \\ &\quad + \int_{\partial\Omega_R^-} [-\dot{\mathbf{y}} \cdot (\mathbf{P} + \boldsymbol{\Sigma}_{\text{MW}})\mathbf{n} + (\mathbf{J} \cdot \mathbf{n})(\mu + q\xi)] \geq 0\end{aligned} \tag{32}$$

To be consistent with (13)–(14) and guarantee $\dot{D} \geq 0$, as in the preceding section, we identify the following through the usual Coleman–Noll type arguments:

(i) Nonnegative rate of dissipation

$$-\mathbf{J} \cdot \nabla(\mu + q\xi) \geq 0. \tag{33}$$

(ii) Instantaneous interior mechanical balance:

$$\mathrm{div}(\mathbf{P}+\boldsymbol{\Sigma}_{\mathrm{MW}})=0 \quad \text{in } \Omega_R. \tag{34}$$

(iii) Boundary conditions:

$$(\mathbf{P}+\boldsymbol{\Sigma}_{\mathrm{MW}})\mathbf{n}-\mathbf{t}^e=0 \quad \text{on } S_N, \qquad \begin{cases} \mu^e+q\xi^e=\mu+q\xi & \text{on } \Upsilon_D, \\ \mathbf{J}\cdot\mathbf{n}=0 & \text{on } \partial\Omega_R\setminus\Upsilon_D. \end{cases} \tag{35}$$

A constitutive response that is consistent with the Second of Law of Thermodynamics(i.e. (33)) and arguably represents the most conventional and simplest choice is the linear mobility/diffusion:

$$\mathbf{v}=-\gamma(\mathbf{x})\nabla(\mu+q\xi), \qquad \mathbf{J}=c\mathbf{v} \qquad \text{in } \Omega_R. \tag{36}$$

For a linearized theory we expand the free energy density at a reference equilibrium state up to quadratic terms for each of the phases.[17]:

$$\begin{aligned}\Psi(\mathbf{F},c;\mathbf{x})\approx&\frac{1}{2}(\mathbf{F}-\mathbf{I})\cdot\mathbb{C}(\mathbf{x})(\mathbf{F}-\mathbf{I})+\alpha_{\mathrm{el}}(c-c_0(\mathbf{x}))\mathrm{Tr}(\mathbf{F}-\mathbf{I})\\ &+\frac{\beta(\mathbf{x})}{2}(c-c_0(\mathbf{x}))^2+\hat{\mu}(\mathbf{x})(c-c_0(\mathbf{x}))+\Psi(\mathbf{I},c_0;\mathbf{x}),\end{aligned} \tag{37}$$

where $\mathbf{I}$ is the identity matrix, $\hat{\mu}$ denotes the chemical potential of the pure ion and is often referred to as the standard chemical potential, and $\mathbb{C}$ is the fourth-order elasticity tensor satisfying the usual major and minor symmetries: $\mathbb{C}_{ijkl}=\mathbb{C}_{klij}=\mathbb{C}_{ijlk}$. From microscopic consideration of polymeric solid electrolytes, we anticipate that $|\mathbb{C}|\sim k_BTn_a$ (n_a-active chains density, k_B-Boltzmann constant, T-absolute temperature) (Hong et al., 2010), and the coupling coefficient $\alpha_{\mathrm{el}}\sim -k_BT$. For ideal dilute liquid solvents of ions, the free energy density $\Psi(c)=k_BTc\log(c/c_0)$, giving rise to:

$$\beta=\frac{k_BT}{c}\Big|_{c=c_0}, \qquad \hat{\mu}=k_BT(\log c/c_0+1)\Big|_{c=c_0}=k_BT. \tag{38}$$

For solid electrolytes, we expect different behavior. Nevertheless, the order of magnitude of these coefficients should be consistent with (38).

By (8), (34), and $(35)_1$, for the simplified free energy density function (37) we have the boundary value problem for mechanical balance:

$$\begin{cases}\mathrm{div}(\mathbf{P}+\boldsymbol{\Sigma}_{\mathrm{MW}})=0, \quad \mathbf{P}=\mathbb{C}(\mathbf{x})\nabla\mathbf{u}+\alpha_{\mathrm{el}}(\mathbf{x})(c-c_0(\mathbf{x}))\mathbf{I} & \text{in } \Omega_R,\\ (\mathbf{P}+\boldsymbol{\Sigma}_{\mathrm{MW}})\mathbf{n}-\mathbf{t}^e=0 & \text{on } S_N,\\ \mathbf{u}=\mathbf{u}^e & \text{on } S_D,\end{cases} \tag{39}$$

Also, the diffusion equation of ion concentration evolution is given by:

$$\begin{cases}\dot{c}+\mathrm{div}\mathbf{J}=0, \quad \mathbf{J}=-c\gamma(\mathbf{x})\nabla(\mu+q\xi) & \text{in } \Omega_R,\\ \mu=\mu^e & \text{on } \partial\Omega_R,\end{cases} \tag{40}$$

where by (37) the chemical potential is given by

$$\mu(\mathbf{x})=\alpha_{\mathrm{el}}(\mathbf{x})\nabla\cdot\mathbf{u}+\beta(\mathbf{x})(c-c_0(\mathbf{x}))+\hat{\mu}(\mathbf{x}). \tag{41}$$

In summary, Eqs. (39), (21) and (40) form a closed coupled partial differential system for $(\mathbf{u},c,\xi)$.

3. Homogenization of composite electrolytes

The coupled boundary value problem in (21), (39) and (40) is nonlinear for $(\mathbf{u},c,\xi)$. Thus, solving it is a challenge even for simple geometries, let alone that we are interested in solving this boundary value problem for heterogeneous systems. In a first step, to gain some insights, we neglect the coupling with elasticity and solve the coupled electro-diffusion system for laminar structures. Based on the analytical solutions to the laminar structures, we propose some approximations for the homogenization of more general microstructures.

3.1. A simplified electro-diffusion model

Our general electro-elastic-diffusion model (21), (39) and (40) can be specified to include some of the classical models including the Poisson–Boltzmann–Nernst–Planck (PBNP) model for electro-diffusion. To see it, we introduce the electrochemical potential

$$\phi=\mu+q\xi,$$

---

[17] For the case of incompressible neo-Hookean solid please refer to the Appendix B.

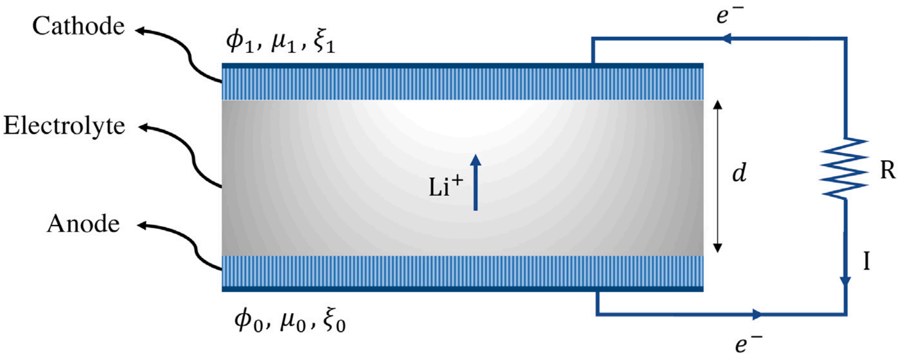

Fig. 4. Schematic of a battery-like system with a homogeneous electrolyte.

and the *Deybe length*

$$\lambda = \sqrt{\frac{\epsilon_0 \beta}{q^2}}. \tag{42}$$

By (41) we have

$$c - c_0 = \frac{1}{\beta}(\phi - q\xi - \hat{\mu} - \alpha_{\mathrm{el}} \nabla \cdot \mathbf{u}). \tag{43}$$

Physically, it is more transparent to rewrite (21), (39), and (40) as a system for $(\xi, \mathbf{u}, \phi)$:

$$\begin{cases} \mathrm{div}(-\epsilon_r(\mathbf{x}) J \mathbf{C}^{-1} \nabla \xi) + \frac{1}{\lambda^2}\xi = \frac{q}{\epsilon_0 \beta}(\phi - \hat{\mu} - \alpha_{\mathrm{el}} \nabla \cdot \mathbf{u}) & \text{in } \Omega_R, \\ \mathrm{div}(\mathbf{P} + \boldsymbol{\Sigma}_{\mathrm{MW}}) = 0 & \text{in } \Omega_R, \\ \mathrm{div}[-\gamma c \nabla \phi] = \dot{c} & \text{in } \Omega_R. \end{cases} \tag{44}$$

We observe that for any constants $(\xi_0, \hat{\mu}_0)$, the system (44) is invariant under the transformation

$$(\xi, \mathbf{u}, \phi; \hat{\mu}) \to (\xi + \xi_0, \mathbf{u}, \phi + q\xi_0 + \hat{\mu}_0; \hat{\mu} + \hat{\mu}_0), \tag{45}$$

implying that an overall constant shift in electric potential or chemical potential does not have any physical consequence.

For small strains with $|\nabla \mathbf{u}| \ll 1$ and under appropriate scaling assumption, we may keep only the leading-order contribution of deformation in $(44)_1$, neglect the Maxwell stress in $(44)_2$, and arrive at a simplified system for $(\xi, \mathbf{u}, \phi)$:

$$\begin{cases} \mathrm{div}(-\epsilon_r \nabla \xi) + \frac{1}{\lambda^2}\xi = \frac{q}{\epsilon_0 \beta}(\phi - \hat{\mu} - \alpha_{\mathrm{el}} \nabla \cdot \mathbf{u}) & \text{in } \Omega_R, \\ \mathrm{div}[\mathbb{C}\nabla \mathbf{u} + \frac{\alpha_{\mathrm{el}}}{\beta}(\phi - q\xi - \hat{\mu} - \alpha_{\mathrm{el}} \nabla \cdot \mathbf{u})\mathbf{I}] = 0 & \text{in } \Omega_R, \\ \mathrm{div}[-\gamma c \nabla \phi] = \dot{c} & \text{in } \Omega_R. \end{cases} \tag{46}$$

If the coupling with elasticity is neglected (i.e., setting $\alpha_{\mathrm{el}} = 0$), we can rewrite (46) as a system for (ξ, ϕ):

$$\begin{cases} \mathrm{div}(-\epsilon_r \nabla \xi) + \frac{1}{\lambda^2}\xi = \frac{q}{\epsilon_0 \beta}(\phi - \hat{\mu}) & \text{in } \Omega_R, \\ c - c_0 = \frac{1}{\beta}(\phi - q\xi - \hat{\mu}) & \text{in } \Omega_R, \\ \mathrm{div}[-\gamma c \nabla \phi] = \dot{c} & \text{in } \Omega_R. \end{cases} \tag{47}$$

We may recognize that the above system is precisely the PBNP model for coupled electro-diffusion (Zheng and Wei, 2011), where the Deybe length λ is the screening length for electrostatic interactions. The Deybe length will pay an important role in our homogenization analysis since the microstructure length-scale l, in general, may be much smaller, comparable, or much larger than λ. We expect distinct effects of microstructure in these regimes.

3.2. Ionic conductivity: definitions and approximations

To demonstrate the fundamental behavior of the PBNP system (46) and lay a ground for homogenization of composite electrolytes with general microstructures, we consider a simple one-dimensional and homogeneous electrolyte body as sketched in Fig. 4. As we will show shortly, even a homogeneous electrolyte displays a complex and rich behavior. Suppose that the resistance in the external circuit is R and the electrical potential difference between two charge collectors is $\triangle\xi (= \xi_1 - \xi_0)$. The electrodes (i.e., the cathode and anode) are electron conductive and consist of active materials that have different chemical potential for the mobile ions, say, Li^+. The geometric changes of electrodes at the contact interfaces are neglected during the charging and discharging processes, though the chemical reactions, depletion and deposition of materials, and morphology changes across the interfaces between electrodes and electrolytes dictate the overall performance of the battery. From this viewpoint, we are only interested in the "instantaneous" ionic conductivity of the electrolytes.

Denote the electrochemical potential, electric potential, and chemical potential on the two electrodes respectively by ϕ_1, ξ_1, μ_1 on the cathode, and ϕ_0, ξ_0, μ_0 on the anode. Then the total current in the external circuit is $I = \triangle\xi/R$. The ionic current density in the electrolyte is uniform and given by I/A (i.e., ion flux $J = I/qA$), where A is the normal area of the electrode in contact with the electrolyte. Consequently, by (47) we have that for steady-states with $\dot{c} \equiv 0$,

$$\begin{cases} -\lambda^2(\epsilon_r \xi')' + \xi = \frac{1}{q}(\phi - \hat{\mu}) & \text{in } \Omega_R, \\ c - c_0 = \frac{1}{\beta}(\phi - q\xi - \hat{\mu}) & \text{in } \Omega_R, \\ -\gamma c \phi' = J & \text{in } \Omega_R. \end{cases} \tag{48}$$

For open circuit, $R \to +\infty$, $J = 0$ and a solution to (48) represents an equilibrium configuration of the system. Based on the invariance (45), without loss of generality we assume $\phi = q\xi + \mu = 0$. Then $(48)_1$ can be written as

$$\mu'' - \frac{1}{\lambda^2 \epsilon_r}\mu = -\frac{1}{\lambda^2 \epsilon_r}\hat{\mu} \qquad \forall\, x \in (0, d), \tag{49}$$

where d is the thickness of the electrolyte layer. For prescribed boundary conditions $\mu(x = 0) = \mu_0 + \hat{\mu}$ and $\mu(x = d) = \mu_1 + \hat{\mu}$, the solution to (49) is explicitly given by ($\lambda_r^2 = \lambda^2 \epsilon_r$ and $\eta = e^{-d/\lambda_r}$)

$$\mu(x) - \hat{\mu} = -q\xi(x) - \hat{\mu} = \frac{\mu_0 - \eta\mu_1}{1 - \eta^2} e^{-x/\lambda_r} + \frac{-\eta\mu_0 + \mu_1}{1 - \eta^2} e^{(x-d)/\lambda_r}, \tag{50}$$

and hence

$$c(x) - c_0 = \frac{1}{\beta}(\mu(x) - \hat{\mu}) = \frac{1}{\beta}[\frac{\mu_0 - \eta\mu_1}{1 - \eta^2} e^{-x/\lambda_r} + \frac{-\eta\mu_0 + \mu_1}{1 - \eta^2} e^{(x-d)/\lambda_r}]. \tag{51}$$

Next, we consider a non-equilibrium process with ionic flux J and external electrical current $I = qJA$. By definition, the *ionic conductivity* K of the electrolyte shall satisfy

$$J = -K\frac{\triangle\phi}{d}. \tag{52}$$

The electrical potential difference between two electrodes satisfies the Ohm's law for the external circuit:

$$\triangle\xi = IR = qJAR.$$

Consequently, the chemical potential difference between cathode and anode is given by

$$\triangle\mu = \mu_1 - \mu_0 = \triangle\phi - q\ \triangle\xi = -(\frac{d}{KA} + q^2 R)AJ. \tag{53}$$

The cathode and anode materials determine the chemical potential difference $\triangle\mu$ which should be taken as a material constant. The efficiency of the overall circuit can be defined as the ratio between the external power (consumed by the external resistor) and the total power output (due to the stored chemical energy):

$$\eta = \frac{I\ \triangle\xi}{-\triangle\mu I/q} = \frac{Rq^2}{q^2 R + d/KA} = 1 - \frac{1}{1 + q^2 RKA/d}. \tag{54}$$

We now consider the problem of how to determine the ionic conductivity. From the definition (52), we necessarily consider a non-equilibrium process with a transport ionic current $J \neq 0$. In this case, the coupled PBNP system (48) is nonlinear and not amenable to closed-form solutions. Nevertheless, we can estimate the influence of the transport ionic current on the profile of chemical potential and mobile ionic concentration. From $(48)_3$, we have

$$\triangle\phi = \phi_1 - \phi_0 = -\frac{Jd}{K} = -\int_0^d \frac{J}{\gamma c} dx. \tag{55}$$

From (49)–(51), we see that the ionic concentration deviates from the natural concentration c_0, and is driven by the chemical potential on the boundary, which influences the overall ionic conductivity via (55). By (53) and (54), we see that $\triangle\phi = (1 - \eta)\ \triangle\mu$. Therefore, if

$$1 - \eta \ll 1, \quad \text{i.e.,} \quad R \gg \frac{d}{q^2 KA}, \tag{56}$$

we may safely neglect the change of concentration $\tilde{c}$ due to the transport ionic current and assume the mobile ion concentration remains close to the equilibrium concentration (51):

$$-\phi' = \frac{J}{\gamma(c + \tilde{c})} \approx \frac{J}{\gamma c} \quad \Rightarrow \quad \triangle\phi \approx -J\int_0^d \frac{1}{\gamma c(x)} dx. \tag{57}$$

Therefore, the *ionic conductivity* K defined by (52) is given by

$$K = \Big[\frac{1}{d}\int_0^d \frac{1}{\gamma c(x)} dx\Big]^{-1}, \tag{58}$$

where $c(x)$ is the equilibrium ionic concentration (given by (51) for the system configuration in Fig. 4).

It is desirable to simplify the result (58) based on the geometric features of the system. There are three different scenarios.

(i) If the overall size of the body is much greater than the Debye length ($d \gg \lambda_r$), we have $\eta = e^{-d/\lambda_r} \ll 1$, $\mu(x) \approx \mu_0 e^{-x/\lambda_r} + \mu_1 e^{(x-d)/\lambda_r}$, and hence by (51),

$$c(x) - c_0 \approx \frac{1}{\beta}\Big[\mu_0 e^{-x/\lambda_r} + \mu_1 e^{(x-d)/\lambda_r}\Big]. \tag{59}$$

From the above expression, we see that the interior ion concentration $c(x) \approx c_0$ except at an interface layer of thickness λ_r which, together with the neutralizing charges on the electrode, is referred to as the double layer. Therefore,

$$\begin{aligned}\gamma c_0 K^{-1} &= \frac{1}{d}\int_0^d \frac{1}{1 + \frac{\mu_0}{\beta c_0}e^{-x/\lambda_r} + \frac{\mu_1}{\beta c_0}e^{(x-d)/\lambda_r}}dx \\ &= 1 - \frac{\lambda_r}{d}\int_0^{d/\lambda_r} \frac{\frac{\mu_0}{\beta c_0}e^{-y} + \frac{\mu_1}{\beta c_0}e^{y-d/\lambda_r}}{1 + \frac{\mu_0}{\beta c_0}e^{-y} + \frac{\mu_1}{\beta c_0}e^{y-d/\lambda_r}}dy \\ &\approx 1 - \frac{\lambda_r}{d}\log(1 + \frac{\mu_0}{\beta c_0})(1 + \frac{\mu_1}{\beta c_0}).\end{aligned} \tag{60}$$

Therefore,

$$K = \Big[\frac{1}{d}\int_0^d \frac{1}{\gamma c(x)}dx\Big]^{-1} \approx \gamma c_0. \tag{61}$$

We remark that this is the typical scenario in applications.

(ii) Though it is unlikely in battery applications, for completeness we may assume $d \ll \lambda_r$, and hence by (51),

$$c(x) - c_0 \approx \frac{1}{\beta}(\frac{d-x}{d}\mu_0 + \frac{x}{d}\mu_1).$$

Therefore,

$$K = \Big[\frac{1}{d}\int_0^d \frac{1}{\gamma c(x)}dx\Big]^{-1} \approx \frac{\gamma(\mu_1 - \mu_0)}{\beta}\Big[\log\Big(\frac{\beta c_0 + \mu_1}{\beta c_0 + \mu_0}\Big)\Big]^{-1}. \tag{62}$$

(iii) If $d \sim \lambda_r$, there is no obvious way to achieve an approximate solution and we would have to numerically evaluate the ionic conductivity by the integral in the first line of (60).

3.3. Homogenization: approximations and unit cell problems

In this section we consider composite electrolytes with general microstructure and outline the homogenization procedure and approximations. For simplicity, we first focus on the PBNP system (47) and assume periodic microstructure in the sense that the relevant material properties are given by

$$(\epsilon_r^{(l)}(\mathbf{x}), \beta^{(l)}(\mathbf{x}), \gamma^{(l)}(\mathbf{x}), \hat{\mu}^{(l)}(\mathbf{x}), c_0^{(l)}(\mathbf{x})) = (\epsilon_r^{\#}(\frac{\mathbf{x}}{l}), \beta^{\#}(\frac{\mathbf{x}}{l}), \gamma^{\#}(\frac{\mathbf{x}}{l}), \hat{\mu}^{\#}(\frac{\mathbf{x}}{l}), c_0^{\#}(\frac{\mathbf{x}}{l})), \tag{63}$$

where $\tilde{\mathbf{x}} \mapsto (\epsilon_r^{\#}(\tilde{\mathbf{x}}), \beta^{\#}(\tilde{\mathbf{x}}), \gamma^{\#}(\tilde{\mathbf{x}}), \hat{\mu}^{\#}(\tilde{\mathbf{x}}), c_0^{\#}(\tilde{\mathbf{x}}))$ are periodic functions with unit cell $C = [0,1)^3$ and $l \ll d$ is the length-scale of the microstructures of the composite. Our goal is to define the effective ionic conductivity of the composite electrolyte as useful characteristics of the macroscopic properties of the overall structure. As a coupled nonlinear system for (ξ, ϕ), the PBNP system (47) is not easily amenable to rigorous analysis. Nevertheless, based on our solution to the one dimensional problem discussed in Section 3.2 we are motivated to make the assumption that the local ionic conductivity, i.e., γc in $(47)_2$, may be assumed to be independent of the transport current as long as the transport current is such that (56) is satisfied. In other words, the chemical energy is mostly converted into work on the external circuit in a discharging process instead of being dissipated into heat due to the resistance of the electrolyte. This is generally necessary for normal applications unless the battery is short-circuited.

For the equilibrium state, by (45) and without loss of generality we set $\phi = q\xi + \mu \equiv 0$ and, by $(47)_1$, obtain a boundary value problem for μ:

$$\begin{cases}\mathrm{div}(-\epsilon_r^{(l)}\nabla\mu) + \frac{1}{(\lambda^{(l)})^2}\mu = \frac{1}{(\lambda^{(l)})^2}\hat{\mu}^{(l)} & \text{in } \Omega_R, \\ \mu = \mu^e & \text{on } \partial\Omega_R,\end{cases} \tag{64}$$

where, for simplicity, a Dirichlet-type boundary condition is assumed for the entire boundary of Ω_R, and material properties $(\epsilon_r^{(l)}, \lambda^{(l)}, \hat{\mu}^{(l)})$ take the form of (63). As a linear differential equation, the solution to (64) can be written as a superposition of two solutions:

$$\mu(\mathbf{x}) = \bar{\mu}(\mathbf{x}) + \mu_p(\mathbf{x}),$$

where μ_p and $\bar{\mu}$ are respectively the solution to

$$\begin{cases}\mathrm{div}(-\epsilon_r^{(l)}\nabla\mu_p) + \frac{1}{(\lambda^{(l)})^2}\mu_p = \frac{1}{(\lambda^{(l)})^2}\hat{\mu}^{(l)} & \text{in } \Omega_R, \\ \mu_p \text{ is periodic with period } [0,l)^3,\end{cases} \tag{65}$$

and

$$\begin{cases} \operatorname{div}(-\epsilon_r^{(l)}\nabla\bar{\mu}) + \frac{1}{(\lambda^{(l)})^2}\bar{\mu} = 0 & \text{in } \Omega_R, \\ \bar{\mu} = \mu^e - \mu^\# & \text{on } \partial\Omega_R. \end{cases} \tag{66}$$

Upon change of variables $\mathbf{x} \to \tilde{\mathbf{x}} = \mathbf{x}/l$ and rescaling $\mu^\#(\tilde{\mathbf{x}}) = \mu_p(l\tilde{\mathbf{x}})$, (65) can be rewritten as a unit cell problem (c.f., (63)):

$$\begin{cases} \operatorname{div}_{\tilde{\mathbf{x}}}(-\epsilon_r^\#\nabla_{\tilde{\mathbf{x}}}\mu^\#) + \frac{l^2}{(\lambda^\#)^2}\mu^\# = \frac{l^2}{(\lambda^\#)^2}\hat{\mu}^\# & \text{in } C = [0,1)^3, \\ \text{periodic boundary condition} & \partial C, \end{cases} \tag{67}$$

where the subscript $_{\tilde{\mathbf{x}}}$ implies partial derivatives with respect to $\tilde{\mathbf{x}}$, and hence $\nabla = \frac{1}{l}\nabla_{\tilde{\mathbf{x}}}$ and $\operatorname{div} = \frac{1}{l}\operatorname{div}_{\tilde{\mathbf{x}}}$.

Based on the exact solution (c.f., (50)) in one dimension, it is widely accepted that the solution to (66) decays exponentially to zero away from the boundary $\partial\Omega_R$ as $\lambda \to 0$ though, to our best knowledge, a rigorous proof cannot be found in the literature. Therefore, we may neglect the contribution of $\bar{\mu}(\mathbf{x})$ in evaluating the local ionic concentration by $(47)_2$ and obtain

$$c(\mathbf{x}) - c_0^\#(\mathbf{x}/l) \approx \frac{1}{\beta^\#(\mathbf{x}/l)}(\mu^\#(\mathbf{x}/l) - \hat{\mu}^\#(\mathbf{x}/l)) \qquad \forall\, \mathbf{x} \in \Omega_R, \tag{68}$$

where $\mu^\#$ is the solution to the unit cell problem (67).

Since the dependence of ionic concentration on the transport current is neglected, the effective ionic conductivity of the periodic composite can be found by the classical homogenization procedure (Milton and Sawicki, 2003). In particular, the effective ionic conductivity tensor $\mathbf{K}^{\text{eff}}$ can be variationally defined as

$$\mathbf{e}\cdot\mathbf{K}^{\text{eff}}\mathbf{e} = \min_{\text{periodic } \phi}\int_C K^\#(\tilde{\mathbf{x}})|\nabla\phi + \mathbf{e}|^2 \qquad \forall\, \mathbf{e} \in \mathbb{R}^3. \tag{69}$$

where

$$K^\#(\tilde{\mathbf{x}}) := \gamma^\#(\tilde{\mathbf{x}})c(l\tilde{\mathbf{x}}) = \gamma^\#(\tilde{\mathbf{x}})[c_0^\#(\tilde{\mathbf{x}}) + \frac{1}{\beta^\#(\tilde{\mathbf{x}})}(\mu^\#(\tilde{\mathbf{x}}) - \hat{\mu}^\#(\tilde{\mathbf{x}}))]. \tag{70}$$

Below we summarize the approximations and procedure to achieve the effective ionic conductivity of the periodic composite electrolytes. The same procedure will be applied to address the coupled electro-elastic-diffusion system (46).

1. Under the open circuit condition, we find the equilibrium chemical potential of the system by (64). The presence of heterogeneities, in particular, the differences of intrinsic chemical potential $\hat{\mu}$ of constituent phases induce electric fields across interfaces that are balanced by the actual chemical potential μ so that the total electrochemical potential $\phi = \mu + q\xi$ vanishes. The actual chemical potential μ could be significantly different from the intrinsic chemical potential $\hat{\mu}$, and hence induce a change of equilibrium ionic concentration by $(47)_2$:

$$c - c_0 = \frac{1}{\beta}(\mu - \hat{\mu}). \tag{71}$$

2. For periodic composite electrolytes with material properties specified by (63), if the Debye length of constituent materials $\lambda^{(l)} \ll d$ (d is the lengthscale of the overall composite body), we may safely neglect the boundary effects and focus on the unit cell problem (65) or (67) to obtain the chemical potential and the local equilibrium ionic concentration by (68).
3. Finally, we consider the non-equilibrium processes and in particular, the diffusion equation $(47)_3$. The variation of ionic concentration due to nonzero $\nabla\phi$ is negligible if (56) is satisfied or at the normal working condition of a battery. Then $(47)_3$ can be recognized as the usual conduction equation with local ionic conductivity $\gamma(\mathbf{x})c(\mathbf{x}) = K^\#(\mathbf{x}/l)$ (c.f., (70)). If the microstructure lengthscale $l \ll d$, from the classic homogenization theory we can determine the macroscopic effective ionic conductivity by the variational problem (69).

3.4. Rigorous bounds

Once the concentration of mobile ions are determined for the equilibrium state under open circuit condition, the local ionic conductivity of electrolyte is given by (70). As is well-known in the theory of composites, the effective ionic conductivity of composite is defined by (69) and then satisfies some rigorous bounds. Suppose the effective composite is isotropic with $\mathbf{K}^{\text{eff}} = K^{\text{eff}}\mathbf{I}$. Then the effective ionic conductivity K^{eff} satisfies the classical Voigt–Reuss bounds:

$$\bar{H} \le K^{\text{eff}} \le \bar{K},$$

where $\bar{H}$ and $\bar{K}$ are respectively the harmonic mean and arithmetic mean of local ionic conductivity:

$$\bar{H} = \langle\frac{1}{K^\#}\rangle^{-1} := \left[\int_C \frac{1}{K^\#(\tilde{\mathbf{x}})}d\tilde{\mathbf{x}}\right]^{-1}, \qquad \bar{K} = \langle K^\#\rangle := \int_C K^\#(\tilde{\mathbf{x}})d\tilde{\mathbf{x}}. \tag{72}$$

Here and subsequently, $\langle(\cdot)\rangle$ denotes the volumetric average of the quantity $(\cdot)$ over the unit cell C.

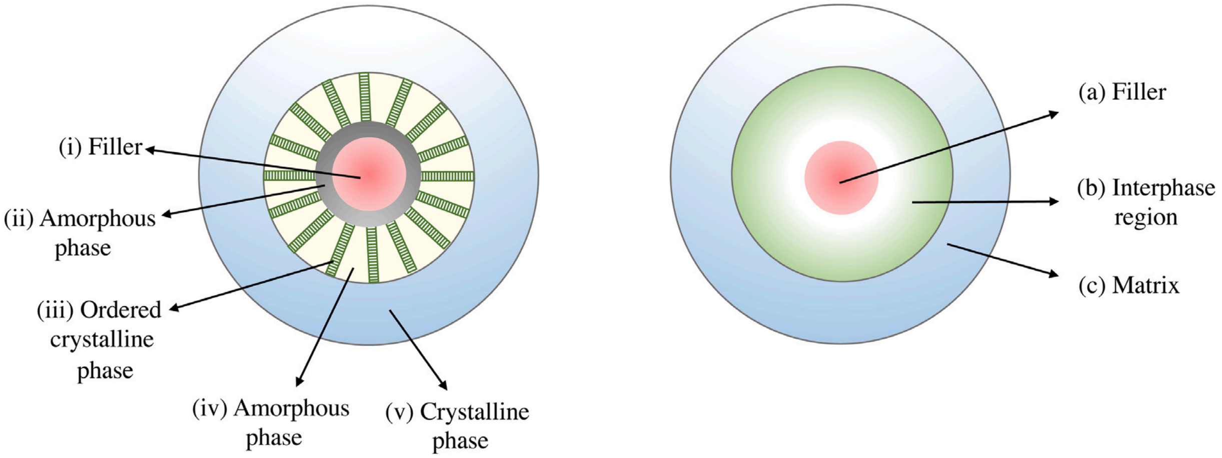

Fig. 5. (Left) Schematic of the typical microstructure of a composite polymer electrolyte. (Right) Simplified microstructure modeled in this work.

Much tighter bounds for K^{eff} can be obtained by the Hashin–Shtrikman's variational principle (Hashin and Shtrikman, 1962b,a, 1963). The Hashin–Shtrikman's bounds for continuously varying local conductivity can be conveniently derived following the argument of Liu (2010) and written as follows:

$$K_L + \frac{nK_L\Gamma_L}{1-\Gamma_L} \le K^{\text{eff}} \le K_U + \frac{nK_U\Gamma_U}{1-\Gamma_U},$$

where $n = 2$ or 3 is the dimension of space, and

$$K_L = \min_{\tilde{\mathbf{x}}\in C} K^{\#}(\tilde{\mathbf{x}}), \qquad K_U = \max_{\tilde{\mathbf{x}}\in C} K^{\#}(\tilde{\mathbf{x}}),$$

$$\Gamma_L = \left\langle \frac{K^{\#}-K_L}{K^{\#}+(n-1)K_U} \right\rangle, \qquad \Gamma_U = \left\langle \frac{K^{\#}-K_U}{K^{\#}+(n-1)K_U} \right\rangle.$$

4. Effective ionic conductivity for some special microstructures

In this section, we find the effective ionic conductivities for a few special microstructures including (a) 1D multilayer solid electrolyte, (b) 3D cylindrical matrix containing rod-like inclusions, and (c) 3D matrix containing spherical inclusions. However, prior to that, in order to be relevant to typical experimental conditions for soft solid electrolytes, we make some key observations about what is known regarding the microstructure of multiphase electrolytes and the associated assumptions we have made in our homogenization models.

4.1. Observations about typical composite electrolyte microstructures and our modeling assumptions

As we have highlighted in the Introduction, typical solid polymer electrolytes suffer from low ionic conductivity due to isotropic crystallinity (Li et al., 2013). Therefore, any attempt to disrupt the isotropic crystallinity usually improves their ionic conductivity (Li et al., 2013). This may be achieved by (i) increasing anisotropic crystallinity which tunes the crystallographic texture (Golodnitsky and Peled, 2000; Minami, 2006) or (ii) generating amorphous regions by disrupting the crystalline structure (Sillamoni and Idiart, 2015).

In our assumptions regarding the microstructure, consistent with our interest in softer solids, we focus on the second notion. This method of enhancing of the ionic conductivity is possible by the addition of nano-particles which disrupt the crystalline structure and the resulting composites often have higher ionic conductivity (Zhang et al., 2020b; Johan et al., 2011; Liu et al., 2015; Wang et al., 2006; Li et al., 2013; Li and Ardebili, 2014). Prior studies have shown that the addition of the fillers act as nucleation sites of growth of spherulite structures[18] (Siekierski et al., 2007) containing the amorphous region and a highly ordered crystalline structure. Both these regions appear to exhibit high ionic mobility (Johan et al., 2011; Sillamoni and Idiart, 2015). In short, the region in the vicinity of fillers have a higher ionic mobility in comparison to the unaltered crystalline polymer (Johan et al., 2011; Sillamoni and Idiart, 2015).

Assuming the filler as the nucleation site for the growth of spherulite structure, the structure around each filler is composed of an amorphous ring followed by lamellar structure containing ordered crystalline polymer distanced around few nanometers from each

---

[18] The spherulite structures are typically in the order of few micrometers or less since they can be restricted by spacing between particles (Wypych, 2012).

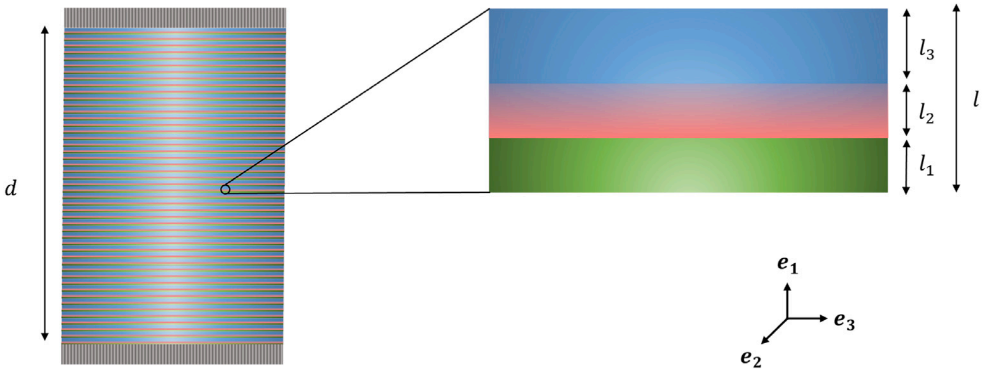

Fig. 6. Schematic of the heterogeneous electrolyte (left) and the unit cell consisting of n layers where we have assumed $n = 3$ for illustration purposes (right).

other and amorphous phases in between, and a crystalline polymer phase around as shown in Fig. 5 (left). For further information we refer the reader to Wypych (2012), Fullerton-Shirey and Maranas (2009).

In this work, we both simplify and (arguably) generalize our thought process. Rather than model the microstructure in Fig. 5 (left) in excruciating detail (which anyway may not hold true for all types of polymer composites), we contend that the simplified microstructure shown in Fig. 5 (right) is quite general and can account (physically) for a diversity of possibilities. The interphase layer simply serves as a proxy for any regional change around the fillers which (usually) is highly conductive. In practice, the thickness of the interphase layer and its properties would require experimental characterization since they would be a function of the involved materials, characteristics of the phases and fabrication process.

4.2. Ionic conductivity of multi-layer electrolytes

As illustrated in Fig. 6, we first consider a multi-layer solid electrolyte. Denote by θ_i the volume fraction and $(\epsilon_r^{(i)}, \sqrt{\frac{\epsilon_0\beta^{(i)}}{q^2}}, \hat{\mu}^{(i)})$ $(i = 1, \dots, n, \sum_{i=1}^{n} \theta_i = 1)$ the relevant material properties of the ith layer. For the equilibrium state under open circuit, by (65) the microscopic periodic chemical potential μ_p satisfies the ordinary differential equation:

$$\begin{cases} -(\epsilon_r(y)\mu_p')' + \frac{1}{\lambda^2(y)}\mu_p = \frac{\hat{\mu}(y)}{\lambda^2(y)} & \forall\, y \in (0, l), \\ \mu_p(0) = \mu_p(l), \qquad \sigma_p(0) = \sigma_p(l) \end{cases} \tag{73}$$

where $\sigma_p(y) := \epsilon_r(y)\mu_p'(y)$, and

$$(\epsilon_r(y), \lambda(y), \hat{\mu}(y)) = \left(\epsilon_r^{(i)}, \sqrt{\frac{\epsilon_0\beta^{(i)}}{q^2}}, \hat{\mu}^{(i)}\right) \qquad \text{if } y \in \text{ the } i\text{th layer.}$$

We use the method of transfer matrix to solve the boundary value problem (73). This method is based on the continuity of the potential and electric displacement across interfaces. Suppose that the values of (μ_p, σ_p) at one end of the jth layer is given by $(\mu^{(j)}, \sigma^{(j)})$. By $(73)_1$ we find that (μ_p, σ_p) at the other end of the layer, denoted by $(\mu^{(j+1)}, \sigma^{(j+1)})$, can be written as

$$\begin{bmatrix} \mu^{(j+1)} \\ \sigma^{(j+1)} \end{bmatrix} = \mathbb{T}^{(j)} \begin{bmatrix} \mu^{(j)} - \hat{\mu}^{(j)} \\ \sigma^{(j)} \end{bmatrix} + \begin{bmatrix} \hat{\mu}^{(j)} \\ 0 \end{bmatrix}, \tag{74}$$

where the transfer matrix $\mathbb{T}^{(j)}$ is given by

$$\mathbb{T}^{(j)} = \frac{1}{2} \begin{bmatrix} \eta + \eta^{-1} & \frac{\lambda_r^{(j)}}{\epsilon_r^{(j)}}(-\eta + \eta^{-1}) \\ \frac{\epsilon_r^{(j)}}{\lambda_r^{(j)}}(-\eta + \eta^{-1}) & \eta + \eta^{-1} \end{bmatrix}, \tag{75}$$

$\eta = e^{-l\theta_j/\lambda_r^{(j)}}$, and $\lambda_r^{(i)} = \sqrt{\frac{\epsilon_0\epsilon_r^{(i)}\beta^{(i)}}{q^2}}$. Imposing the periodic boundary condition $(73)_2$ will determine $(\mu^{(j)}, \sigma^{(j)})$ at the interfaces, and hence the potential $\mu_p(y)$ as

$$\bar{\mu}_p(z(y)) = \hat{\mu}^{(j)} + (\mu^{(j)} - \hat{\mu}^{(j)}) \cosh\left(\frac{z}{\lambda_r^{(j)}}\right) + \frac{\lambda_r^{(j)}\sigma^{(j)}}{\epsilon_r^{(j)}} \sinh\left(\frac{z}{\lambda_r^{(j)}}\right) \qquad \text{in } z \in (0, l\theta_j), \tag{76}$$

where $\bar{\mu}_p(z(y)) := \mu_p(y)$ and z is the local coordinate of each layer defined by:

$$z(y) = y - \left(\sum_{j=1}^{i-1} l\theta_j\right) \qquad \text{if } y \in \text{ the } i\text{th layer.} \tag{77}$$

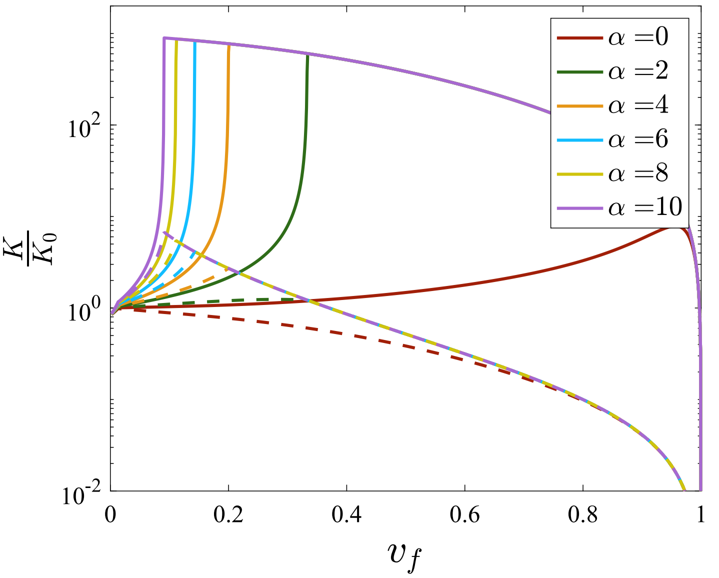

Fig. 7. The normalized ionic conductivity versus the volume fraction of the fillers($v_f := l_1/l$) for various interphase extension factors (α). The ionic conductivity is normalized with the ionic conductivity of the case $v_f = 0$ i.e. the homogeneous matrix. The length of the first layer(filler) is fixed at $l_1 = 2$ nm, $\Delta\hat{\mu} = \hat{\mu}^{(3)} - \hat{\mu}^{(1)} = 1$ eV and $\hat{\mu}^{(2)} = \hat{\mu}^{(3)}$. Solid lines represent active fillers(high mobility) with $\gamma_3 \ll \gamma_2 = \gamma_1 \& \frac{\gamma_2}{\gamma_3} = 1000$ while the dashed lines represent the case of passive fillers(low mobility), i.e. $\gamma_1 = \gamma_3 \ll \gamma_2 \& \frac{\gamma_2}{\gamma_3} = 1000$. In both cases, it is assumed that the initial concentration is zero at the filler phase i.e. $c_0^{(1)} = 0$ mole/m^3 while $c_0^{(2)} = c_0^{(3)} = 50$ mole/m^3. The numerical values are $\lambda_r^{(1)} = \lambda_r^{(2)} = \lambda_r^{(3)} = 4$ nm, $\epsilon_r^{(1)} = 10$ and $\epsilon_r^{(2)} = \epsilon_r^{(3)} = 3$.

By (71) the concentration of the ions in each layer is obtained as:

$$\bar{c}\left(z(y)\right) = c_0^{(j)} + \frac{(\mu^{(j)} - \hat{\mu}^{(j)})}{\beta^{(j)}} \cosh\left(\frac{z}{\lambda_r^{(j)}}\right) + \frac{\lambda_r^{(j)}\sigma^{(j)}}{\beta^{(j)}\epsilon_r^{(j)}} \sinh\left(\frac{z}{\lambda_r^{(j)}}\right) \qquad \text{in } z \in (0, l\theta_j). \tag{78}$$

Consequently, by (69) the ionic conductivity along $\mathbf{e}_1$ is given by the harmonic mean (58) whereas the ionic conductivity in directions perpendicular to $\mathbf{e}_1$ is equal to the arithmetic mean (Milton and Sawicki, 2003):

$$K^{\perp} = \bar{K}, \tag{79}$$

where $\bar{K}$ is defined in (72).

Based on the physical insights in Section 4.1, as a special case, we present results for a three-layer electrolyte, in which the layers are composed of (1) crystalline polymer, (2) an interphase region and (3) ceramic filler. Here, we assume an extension around the filler with length l_{int} and normalize it to the size of the filler layer as

$$l_{\text{int}} = \alpha l_1 = \alpha\theta_1 l,$$

where α is the constant of proportionality and called **interphase extension factor**. We emphasize again that the thickness of the interphase layer is a function of the geometry of the problem, characteristics of the phases and fabrication process.

In the remainder of this section, we present some explicit numerical results. Also the subscripts (superscripts) (1,2,3) in any variable refer to the filler, interphase region and polymer matrix respectively.

Fig. 7 shows the normalized ionic conductivity versus the volume fraction of the filler $v_f := l_1/l$, for different values of α while the size of the filler is kept at $l_1 = 2$ nm. Here, we represent the results for both active fillers (high mobility) as well as passive fillers (low mobility). From this figure, we infer that the ionic conductivity can be enhanced by orders of magnitude by addition of a small amount of fillers with high interphase extension factor. From a physical point of view, we believe that such a scenario corresponds to percolation as reported in the literature (Sillamoni and Idiart, 2015; Do et al., 2012) and the maximum ionic conductivity is obtained in a case where the polymer part of the electrolyte is made up of highly mobile interphase polymer.

Taking a closer look at Fig. 7, we notice an appreciable difference between the enhancement of the ionic conductivity due to addition of active versus passive fillers; while both active and passive fillers form nucleation sites for the formation of amorphous highly mobile polymer phase, active fillers also contribute in the ionic transport and thus more enhancement is observed in the effective ionic conductivity for those.

4.3. Effective ionic conductivity for multilayer solid electrolytes considering mechanical coupling

In the previous section, for simplicity and to gain some insights, we neglected the coupling between electro-diffusion and elasticity. In this section we investigate the effect of the deformation on the electrolyte ionic conductivity. As illustrated in Fig. 8,

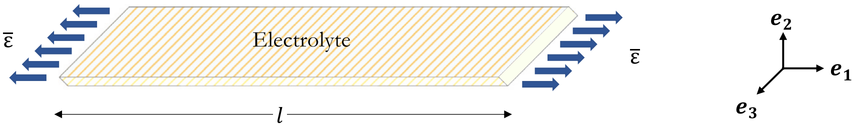

Fig. 8. Schematic of a heterogeneous electrolyte in a 1D setup under average stretch $\bar{\varepsilon}$.

we consider a thin film that is stretched from two ends. For the equilibrium state ($\phi = 0$), from (46) we write the boundary value problem as:

$$\begin{cases} (-\epsilon_r(x)\mu_p')' + \frac{1}{\lambda^2(x)}\mu_p = \frac{1}{\lambda^2(x)}(\hat{\mu}(x) + \alpha_{\mathrm{el}} u') & \text{in } \Omega_R, \\ [P]' = 0 \qquad P = E_y(x)u' + \frac{\alpha_{\mathrm{el}}}{\beta}(\mu_p - \hat{\mu}(x) - \alpha_{\mathrm{el}} u') & \text{in } \Omega_R, \\ u(l) - u(0) = l\bar{\epsilon} & \text{on } S_N, \end{cases} \tag{80}$$

where E_y denotes the elastic modulus of the body and $\bar{\epsilon}$ is the average strain in the body.

After obtaining the chemical potential and displacement from solving the boundary value problem in (80), the concentration of the ions in each layer can be obtained. The ionic conductivity in the direction of the ionic transport can be calculated by (58). In the perpendicular direction, the ionic conductivity can be obtained from (79).

To understand the effect of elasticity on diffusion from another perspective, we now assume that instead of the imposed displacement, tractions are exerted in the boundaries. Due to the 1D nature of the stated problem in (80), the stress P is constant throughout the body. Therefore, $(80)_1$ and $(80)_2$ can be simplified as

$$\mu'' = \frac{1}{\bar{\lambda}_r^2}\left(\mu - \hat{\mu} - \frac{\alpha_{\mathrm{el}} P}{E_y}\right) \tag{81}$$

where $\bar{\lambda}_r^2 = \lambda_r^2\left(1 - \frac{\alpha_{\mathrm{el}}^2/\beta}{E_y}\right)$. From (81), we observe that the coupling with elasticity has an impact on both the effective Debye length and $\hat{\mu}$. In other words, the applied stress impacts the $\hat{\mu}$ of the system in comparison to the case of without stress.

To examine the role of mechanical deformation in the heterogeneous context, similar to previous section, we solve the boundary value problem in (80) for a system consist of three layers of (1) filler, (2) interphase region and (3) the polymer matrix; for various applied strains and obtain the ionic conductivity from (58). Fig. 9 shows the effect of the external loading on the enhancement of the ionic conductivity. For brevity we provided the normalized ionic conductivity as the ratio of the ionic conductivity with applied stress to the case of the ionic conductivity of reference homogeneous system without accounting for this mechanical coupling. In conclusion, stretch can increase ionic conductivity by orders of magnitude since mechanical deformation can increase number of available ions.

It is instructive to delve a little deeper into the origins of the effect of deformation on ionic conductivity. Physically, stretching may increase the ionic conductivity in the following two key ways: (1) The polymer chains get aligned leading to easier pathways for the ions to cross by modifying the mobility of the system; (2) The number of available ions is increased i.e. the equilibrium ionic concentration is shifted due to mechanical deformation. Modeling the first aspect is beyond the scope of our work and may be addressed by characterizing a deformation-dependent mobility. The second mechanism (which is accounted for in our model) is readily understood by a simple toy model. Due to stretching, the configurational entropy of the system increases leading to a reduction in the free energy. This allows a larger number of ions in the equilibrium configuration. For the toy model, just to drive this point home, we just consider a chemo-elastic system (without electrostatics) and a one-dimensional homogeneous body under influence of an imposed strain ϵ and chemically exposed to the air i.e. $\mu = 0$ at two ends. We use the general form of the free energy density at a reference equilibrium in (37). At steady state, the equilibrium concentration is achieved when the free-energy is minimized. Thus, minimizing the energy with respect to the concentration of ions, we obtain

$$\frac{\partial \Psi}{\partial c} = 0 \rightarrow \alpha_{\mathrm{el}} u' + \beta(c_0^{\epsilon} - c_0) = 0. \tag{82}$$

Therefore, the concentration of ions under strained condition can be obtained as

$$c_0^{\epsilon} = -\frac{\alpha_{\mathrm{el}}}{\beta} u' + c_0, \tag{83}$$

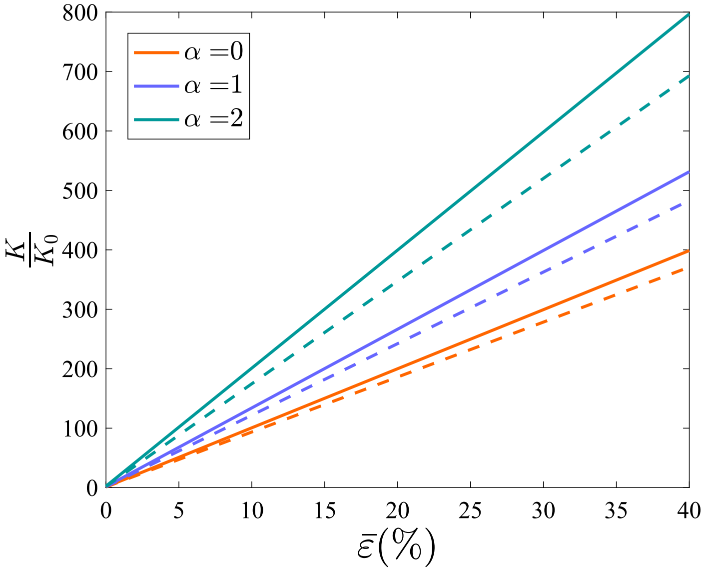

Fig. 9. Normalized enhanced ionic conductivity with respect to the average strain for different interphase extensions. The solid (dashed) lines are for the case of active (passive) fillers. The ionic conductivity is normalized with the case of the homogeneous system. The detailed numerical values are adopted from Fig. 7 caption. Also, $v_f = 0.2$, $\alpha_{\mathrm{el}} = -10^{-16} \times [80, 3, 3]$ J, and $E_y = [70, 0.03, 0.03]$ GPa.

where c_0^ϵ is the equilibrium concentration under strained condition while c_0 (as before) is the equilibrium concentration at zero imposed deformation. Thermodynamics tells us that β must always be positive. The variable α_{el}, in simple terms, measures the increase in volume due to change in concentration. This value can, in principle, be either negative or positive, however, typical materials (e.g. Li-Si system) will swell in volume due to concentration and hence (to the best that we know) this material parameter typically takes negative values. This then necessarily implies that stretching should lead to an *increase* in the number of available ions (i.e. $c_0^\epsilon > c_0$). Accordingly, imposition of a tensile strain on the electrolyte is tied to the increase in the overall concentration of ions in the system and a consequent enhancement of ionic conductivity. A similar conclusion was also reached by Berg et al. (2018) who presented experimental data. We remark that the percentage increase in the equilibrium concentration of ions due to strain scales by the factor $-\frac{\alpha_{\mathrm{el}}}{\beta c_0}$. For typical values of these material parameters, as shown in Section 5, even modest tensile strain values may lead to three orders of magnitude increase in ionic conductivity.

The linear enhancement of the ionic conductivity due to the applied stretch is reported by numerous experiments (Golodnitsky and Peled, 2000; Golodnitsky et al., 2003; Kelly et al., 2016; Minami, 2006) and in Section 5 we will compare our results with the experiments in the literature.

4.4. Effective ionic conductivity of fiber fillers embedded in cylindrical matrix

We now consider a microstructure of where the matrix is populated with cylindrical fibers with radius of $r^{(n)}$, as shown in Fig. 10 for $n = 3$. In analogy with (65) we consider the following problem for the microscopic equilibrium state:

$$\begin{cases} -\operatorname{div}(\epsilon_r(\mathbf{x})\nabla\mu_p) + \dfrac{1}{\lambda^2(\mathbf{x})}\mu_p = \dfrac{1}{\lambda^2(\mathbf{x})}\hat{\mu}(\mathbf{x}) & \text{if } |\mathbf{x}| < r^{(n)}, \\ -\epsilon_r(\mathbf{x})(\nabla\mu_p)\cdot\mathbf{e}_r\Big|_{|\mathbf{x}|=r^{(n)}} = 0. \end{cases} \tag{84}$$

As an example, let the microstructure of the body divided into radial phases in which

$$(\epsilon_r(\mathbf{x}), \lambda(\mathbf{x}), \hat{\mu}(\mathbf{x})) = (\epsilon_r^{(i)}, \sqrt{\frac{\epsilon_0\beta^{(i)}}{q^2}}, \hat{\mu}^{(i)}) \qquad \text{if } |\mathbf{x}| \in [r^{(i-1)}, r^{(i)}),$$

where $r^{(i-1)}$ and $r^{(i)}$ are the inner and outer radius of phase i and $r^{(0)}$ is set to 0.

We assume that the body is very long in the direction of the fibers ($\mathbf{e}_3$) in comparison to the other dimensions of the microstructure. Therefore, the problem can be approximated as plane strain. From the axisymmetric nature of the problem, we set $\mu_p(\mathbf{x}) = \mu_p(r) = F(r) + \hat{\mu}(r)$ where $r = |\mathbf{x}|$ is the magnitude of the position vector on cylindrical coordinate(r, θ, z). Thus, the

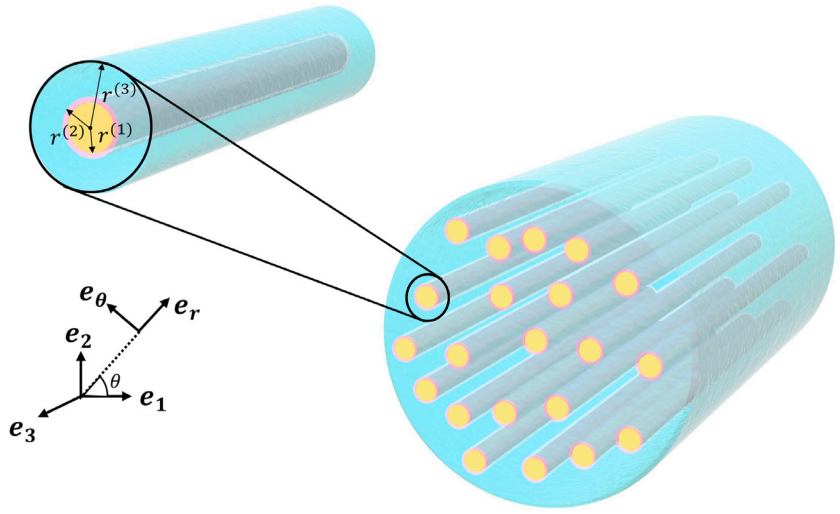

Fig. 10. Schematic of a cylindrical heterogeneous matrix with embedded fibers (right) and the unit cell (left). The unit matrix is assumed to have n phases and here for simplicity we set $n = 3$.

solution in each layer is obtained as:

$$\mu_p(r) = \begin{cases} AJ_0\left(\frac{\imath r}{\lambda_r^{(1)}}\right) + \hat{\mu}^{(1)} & r < r^{(1)}, \\ \\ B_i J_0\left(\frac{\imath r}{\lambda_r^{(i)}}\right) + C_i Y_0\left(-\frac{\imath r}{\lambda_r^{(i)}}\right) + \hat{\mu}^{(i)} & r^{(i-1)} \leq r < r^{(i)} \qquad \text{for } 1 < i \leq n, \end{cases} \tag{85}$$

where $\lambda_r^{(j)} = \sqrt{\frac{\epsilon_0 \epsilon_r^{(j)} \beta^{(j)}}{q^2}}$, $\imath$ is the unit imaginary number and A, B_i and C_i are determined by the boundary and interfacial conditions. Once the chemical potential is obtained, concentration of the ions can be calculated from (71).

In the next step, we calculate the effective ionic conductivity by solving (69). For the microstructure illustrated in Fig. 10, along the fiber direction ($\mathbf{e}_3$), similar to (79) the effective conductivity is given by the arithmetic mean from (72) as:

$$K^{\text{eff}}_{\mathbf{e}_3} := \bar{K} = \int_{\Omega_R} \gamma(r)c(r). \tag{86}$$

On the other hand, the ionic conductivity in the perpendicular direction of the fibers, due to the radial symmetry, can be obtained by solving the boundary value problem as follows:

$$\begin{cases} \text{div}[\mathbf{J}] = 0, \quad \mathbf{J} = -\gamma(r)c(r)\nabla\phi & \text{in } \Omega_R, \\ \phi(\mathbf{x}) = -\bar{E}\mathbf{e}_2 \cdot \mathbf{x} & \text{at } |\mathbf{x}| = r^{(n)}, \end{cases} \tag{87}$$

where for simplicity we are obtaining the ionic flux in $\mathbf{e}_2$ direction and $\bar{E}$ is the magnitude of the electric field applied on the boundaries. We define $f(r)$ such that $\phi(\mathbf{x}) = \nabla f(r) \cdot \mathbf{e}_2$. Therefore, the flux becomes:

$$\mathbf{J} = -\gamma(r)c(r)\left(\frac{\partial^2 f(r)}{\partial r^2}\sin(\theta)\mathbf{e}_r + \frac{1}{r}\frac{\partial f(r)}{\partial r}\cos(\theta)\mathbf{e}_\theta\right). \tag{88}$$

Inserting (88) into (87) and introducing $g(r) = \frac{\partial f(r)}{\partial r}$, we arrive at:

$$\begin{cases} \text{div}[\mathbf{J}] = \left[-\frac{\partial\left(\gamma(r)c(r)\frac{\partial g(r)}{\partial r}\right)}{\partial r} - \frac{1}{r}\left(\gamma(r)c(r)\frac{\partial g(r)}{\partial r}\right) + \frac{1}{r^2}\left(\gamma(r)c(r)g(r)\right)\right]\sin(\theta) = 0, \\ g(r)\Big|_{r=b} = -\bar{E}r^{(n)}, \end{cases} \tag{89}$$

where the continuity conditions at the interfaces are listed as $[\![g(r)]\!]=0$ and $[\![\mathbf{J} \cdot \mathbf{e}_r]\!]=0$. Finally, the ionic conductivity in the perpendicular direction of the fibers is obtained as:

$$K^{\perp} := -\frac{\langle \mathbf{J} \cdot \mathbf{e}_2 \rangle}{\bar{E}}. \tag{90}$$

In the remainder of the section, as a special case, we obtain the ionic conductivity in fiber direction for the case of a three layer system, composed of (1) filler($r^{(1)} = a$), (2) interphase region($r^{(2)} = a(\alpha + 1)$) and (3) the polymer matrix($r^{(3)} = b$) as shown in Fig. 10

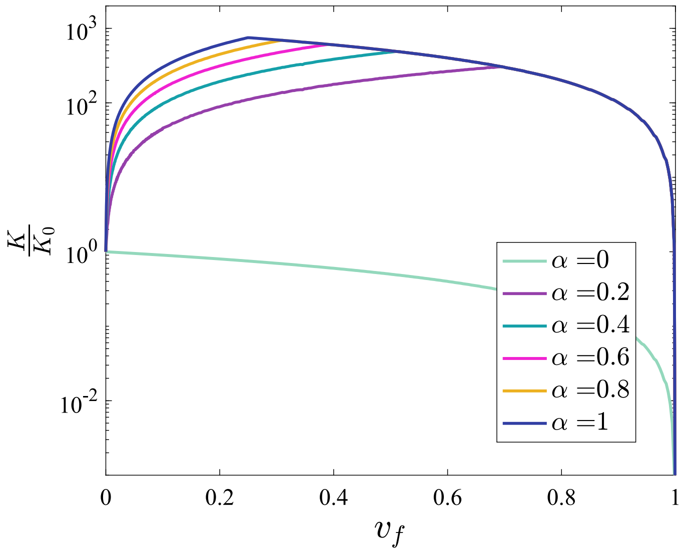

Fig. 11. Normalized ionic conductivity with respect to the volume fraction of the fibers ($v_f := a^2/b^2$) for different interphase extension factors α. The inclusion radius is kept constant at $a = 2$ nm. It is assumed that $\gamma_1 = \gamma_3$ and $\frac{\gamma_2}{\gamma_1} = 1000$, $\Delta\hat{\mu} = \hat{\mu}^{(3)} - \hat{\mu}^{(1)} = 1$ eV, $\hat{\mu}^{(2)} = \hat{\mu}^{(3)}$, $c_0^{(1)} = 0$ mole/m^3, $c_0^{(2)} = c_0^{(3)} = 20$ mole/m^3, $\lambda_r^{(1)} = \lambda_r^{(2)} = \lambda_r^{(3)} = 4$ nm, $\epsilon_r^{(1)} = 10$ and $\epsilon_r^{(2)} = \epsilon_r^{(3)} = 3$.

(left). Similar to the 1D case, and based on the aforementioned physical insights in Section 4.1 we have assumed that there is an extension of highly mobile region around the fillers of thickness l_{int} (—expressed in a normalized fashion with respect to the size of the inclusions as $l_{\text{int}} = \alpha a$). Fig. 11 depicts the enhancement of the ionic conductivity in fiber direction due to the addition of the fillers with volume fraction $v_f := \frac{a^2}{b^2}$ for various interphase extension factors α. We can infer from this figure that the ionic conductivity can be enhanced by orders of magnitude by addition of rod like inclusions in the case of heterogeneous electrolytes. Also, Fig. 12 provides the enhanced ionic conductivity versus the non-dimensionalized variable $\frac{b-a}{l_{\text{int}}}$. We observe that the maximum ionic conductivity is achievable in the state where the polymer matrix is mostly covered by the interphase polymer. The critical size of the inclusion can be obtained as:

$$a_{cr} = b - l_{\text{int}} = \frac{l_{\text{int}}}{\left(\frac{1}{\sqrt{v_f}} - 1\right)}. \tag{91}$$

4.5. Effective ionic conductivity of a heterogeneous electrolyte with spherical inclusions

Consider a heterogeneous solid electrolyte body as shown in Fig. 13 (left). We follow the steps of the homogenization that we discussed in Section 3.3. The microstructure is of radius $r^{(n)}$, as shown in Fig. 13 (right) for $n = 3$. Assuming steady-state and equilibrium($\mathbf{J} = 0$) and neglecting the mechanical effects ($\alpha_{\text{el}} = 0$), by $(47)_1$ we find:

$$\begin{cases} -\operatorname{div}(\epsilon_r(\mathbf{x})\nabla\mu_p) + \dfrac{1}{\lambda^2(\mathbf{x})}\mu_p = \dfrac{1}{\lambda^2(\mathbf{x})}\hat{\mu}(\mathbf{x}) & \text{if } |\mathbf{x}| < r^{(n)}, \\ -\ \epsilon_r(\mathbf{x})(\nabla\mu_p)\cdot\mathbf{e}_r\Big|_{|\mathbf{x}|=r^{(n)}} = 0. & \end{cases} \tag{92}$$

We use separation of variables for solving this problem. We set $\mu_p(\mathbf{x}) = F(r)G(\theta,\phi)$ where $r = |\mathbf{x}|$, θ and ϕ are the magnitudes of $\mathbf{x}$ in the orthogonal basis of the spherical coordinate. Since we have spherical symmetry in this problem the solution can be obtained as:

$$\mu_p(\mathbf{x}) = \mu_p(r) = \begin{cases} \dfrac{A\sinh\left(\frac{r}{\lambda_r^{(1)}}\right)}{r/\lambda_r^{(1)}} + \hat{\mu}^{(1)} & r \le r^{(1)}, \\ \dfrac{B_i\sinh\left(\frac{r}{\lambda_r^{(2)}}\right) + C_i\cosh\left(\frac{r}{\lambda_r^{(i)}}\right)}{r/\lambda_r^{(i)}} + \hat{\mu}^{(i)} & r^{(i-1)} \le r < r^{(i)} \qquad \text{for } 1 < i \le n, \end{cases} \tag{93}$$

where A, B_i and C_i are obtained by the continuity conditions at interfaces and boundary conditions. The concentration of ions will be obtained from (71).

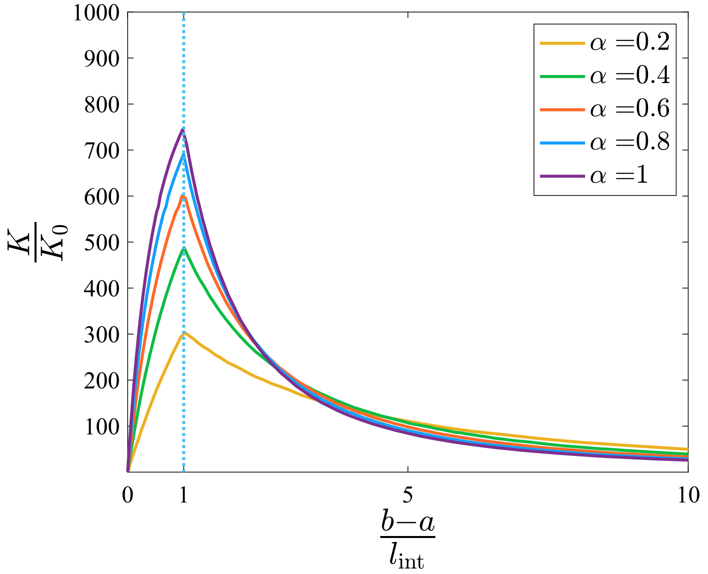

Fig. 12. Normalized ionic conductivity with respect to the dimensionless parameter $\frac{b-a}{l_{\text{int}}}$ for various volume fraction of the filler v_f while the size of the inclusion is kept constant at $a = 2$ nm. The numerical values are $\gamma_1 = \gamma_3$ and $\frac{\gamma_2}{\gamma_1} = 1000$, $\Delta\hat{\mu} = \hat{\mu}^{(3)} - \hat{\mu}^{(1)} = 1$ eV, $\hat{\mu}^{(2)} = \hat{\mu}^{(3)}$, $c_0^{(1)} = 0$ mole/m^3, $c_0^{(2)} = c_0^{(3)} = 20$ mole/m^3, $\lambda_r^{(1)} = \lambda_r^{(2)} = \lambda_r^{(3)} = 4$ nm, $\epsilon_r^{(1)} = 10$ and $\epsilon_r^{(2)} = \epsilon_r^{(3)} = 3$.

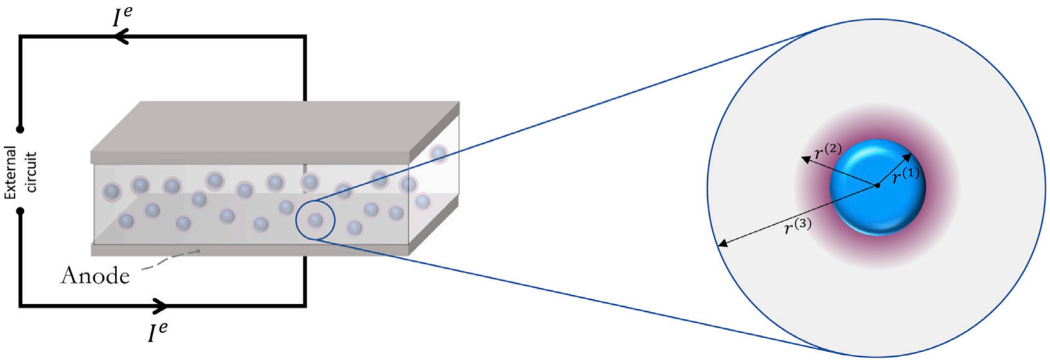

Fig. 13. Schematic of a battery including heterogeneous solid polymer electrolyte (left) and the microscopic unit cell with n radial phases where for illustration purpose we assumed $n = 3$ (right).

Having the concentration of ions in hand, we solve (47)$_3$ for the potential:

$$\begin{cases} \operatorname{div}[\mathbf{J}] = 0, \qquad \mathbf{J} = -\gamma(\mathbf{x})c(\mathbf{x})\nabla\phi & \text{in } \Omega_R, \\ \phi(\mathbf{x}) = -\bar{E}\mathbf{e}_3 \cdot \mathbf{x} & \text{at } |\mathbf{x}| = r^{(n)}. \end{cases} \tag{94}$$

We define $f(r)$ such that $\phi = \nabla f(r) \cdot \mathbf{e}_3$. Inserting it into (94)$_1$ and introducing $g(r) := \frac{\partial f(r)}{\partial r}$, we obtain:

$$\begin{cases} \operatorname{div}[\mathbf{J}] = \frac{1}{r^2}\left(\frac{\partial(-r^2\gamma(r)c(r)\frac{\partial g(r)}{\partial r})}{\partial r} + 2\gamma(r)c(r)g(r)\right)\cos(\theta), \\ \qquad\quad = \frac{-\cos(\theta)}{r^2}\left(r^2\gamma(r)c(r)\frac{\partial^2 g(r)}{\partial r^2} + \frac{\partial(r^2\gamma(r)c(r))}{\partial r}\frac{\partial g(r)}{\partial r} - 2\gamma(r)c(r)g(r)\right) = 0, \\ g(r)\Big|_{r=b} = -\bar{E}r^{(n)}, \end{cases} \tag{95}$$

where the continuity conditions are listed as $[\![g(r)]\!]=0$ and $[\![\mathbf{J} \cdot \mathbf{e}_r]\!]=0$. The ionic conductivity is defined as:

$$K := -\frac{\langle \mathbf{J} \cdot \mathbf{e}_3 \rangle}{\bar{E}}, \tag{96}$$

In the remainder of the section, as a special case, we obtain the ionic conductivity for the case of a three phase system, composed of (1) filler($r^{(1)} = a$), (2) interphase region($r^{(2)} = a(\alpha+1)$) and (3) the polymer matrix($r^{(3)} = b$) as shown in Fig. 13 (right). We assume

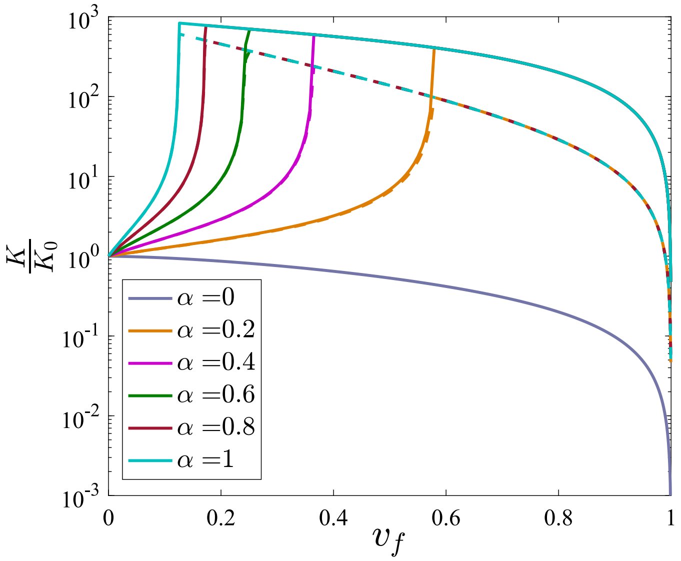

Fig. 14. Normalized ionic conductivity with respect to the volume fraction of the inclusions ($v_f = a^3/b^3$) for different interphase extension factors α. The inclusion size is kept constant as $a = 2$ nm and for the mobility of each layer it is assumed that $\gamma_1 = \gamma_2^{(\theta)} = \gamma_2^{(\theta)} = 1000 \times \gamma_3$ for solid lines and $\gamma_1 = \gamma_3$ and $\gamma_2^{(\theta)} = \gamma_2^{(r)} = 1000 \times \gamma_3$ for dashed lines . Also $\Delta\hat{\mu} = \hat{\mu}^{(3)} - \hat{\mu}^{(1)} = 1$ eV and $\hat{\mu}^{(2)} = \hat{\mu}^{(3)}$, $c_0^{(1)} = 0$ mole/m^3, $c_0^{(2)} = c_0^{(3)} = 20$ mole/m^3 and $\lambda_r^{(1)} = \lambda_r^{(2)} = \lambda_r^{(3)} = 4$ nm for all cases and $\epsilon_r^{(1)} = 10$ and $\epsilon_r^{(2)} = \epsilon_r^{(3)} = 3$.

that the mobility in the interphase region in radial and angular direction can be expressed by $\gamma_2^{(r)}$ and $\gamma_2^{(\theta)}$ which are higher than the mobility of the polymer matrix. In the remainder of this section, we present some of the numerical results.

Fig. 14 shows the normalized ionic conductivity with respect to the volume fraction of the inclusions for both active and passive inclusions, while keeping the size of the inclusion constant. Similar to what we have observed in the 1D case, for each choice of α, by increasing the volume fraction of fillers, we observe a peak and a continuous decrease after that. The interpretation of this observation is as follows: In the first regime, by increasing the volume fraction of the inclusion, the interphase region covers more portions of the polymer matrix. As soon as the interphase covers the whole matrix, we observe a peak in the ionic conductivity. Further increase in the volume fraction would no longer be beneficial to the emergent ionic conductivity due to the decrease in the available ions. A similar trend has been reported in experiments (Johan et al., 2011; Wang et al., 2006). It is worthwhile to mention that the enhancement of the ionic conductivity with active fillers is higher and the reason is simple: while both active and passive inclusions act as nucleation base for the growth of interphase regions, the active inclusions also contribute to the transport of the ions and consequently enhance the ionic conductivity more effectively. In conclusion, the maximum ionic conductivity is obtained from a balance between interphase region extension around added particles and the available ions in the system.

For obtaining the characteristics of the maximum ionic conductivity, we have plotted the normalized ionic conductivity with respect to the dimensionless variable $\frac{b-a}{l_{\text{int}}}$ which indicates a ratio of the polymer phase to the interphase region in Fig. 15. The maximum ionic conductivity is exactly at a point where the interphase region covers all the matrix which is at $\frac{b-a}{l_{\text{int}}} = 1$. Further, the critical size of the inclusion is provided by:

$$a_{cr} = b - l_{\text{int}} = \frac{l_{\text{int}}}{\left(\frac{1}{\sqrt[3]{v_f}} - 1\right)}. \tag{97}$$

5. Connection to experiments

Although we have made scattered remarks in the preceding sections regarding the insights from our model and experiments in the literature, in this section, we make a more systematic comparison and as well compare the various microstructures addressed in our work.

Comparing the improvement in the ionic conductivity for the spherical and cylindrical inclusions in Fig. 16, we infer that the aligned cylindrical inclusions are the most effective way to enhance the ionic conductivity of the composite electrolytes with otherwise similar characteristics. Apart from the higher peak value of the ionic conductivity enhancement in the cylindrical case, there are other drawbacks to the use of the spherical inclusion microstructure that have been observed in experimental setups. For instance, studies reveal that higher fraction of the spherical inclusions have adverse effect on the ionic conductivity for reasons such as increased tortuosity in the transportation path of the ions (Shen and Chen, 2007), ion trapping and pairing and

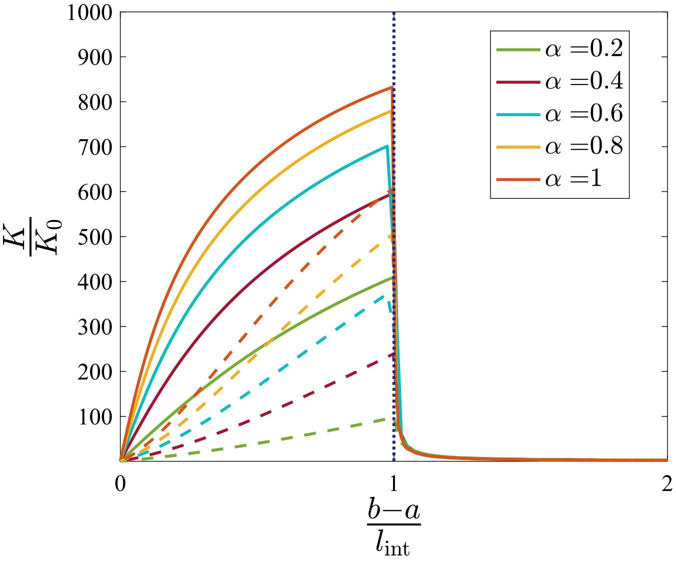

Fig. 15. Normalized ionic conductivity with respect to the dimensionless parameter $\frac{b-a}{l_{\text{int}}}$ for various volume fraction of the filler v_f while the size of the inclusion is kept constant at $a = 2$ nm. The numerical values are $\gamma_1 = \gamma_3$, $\gamma_2^{(\theta)} = \gamma_2^{(r)} = 1000 \times \gamma_1$. Also $\Delta\hat{\mu} = \hat{\mu}^{(3)} - \hat{\mu}^{(1)} = 1$ eV and $\hat{\mu}^{(2)} = \hat{\mu}^{(3)}$, $c_0^{(1)} = 0$ mole/m^3, $c_0^{(2)} = c_0^{(3)} = 20$ mole/m^3 and $\lambda_r^{(1)} = \lambda_r^{(2)} = \lambda_r^{(3)} = 4$ nm for all cases.

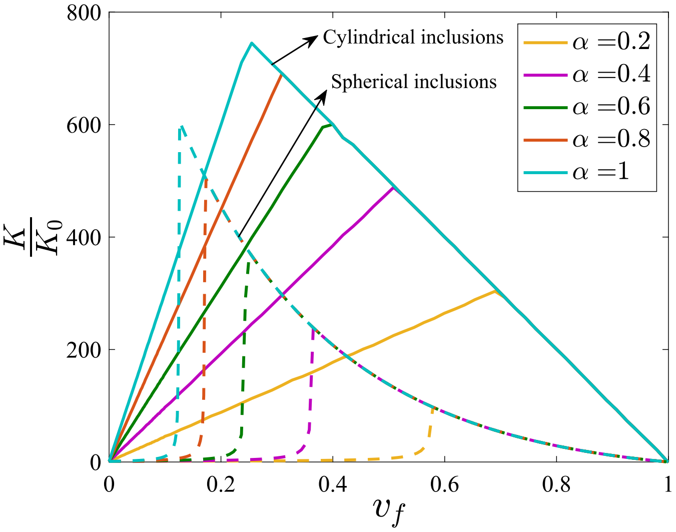

Fig. 16. Comparison of the normalized enhanced ionic conductivity with respect to the volume fraction of the inclusions for cylindrical inclusions (solid lines) and spherical inclusions (dashed lines) for non conductive fillers. The numerical values for cylindrical and spherical inclusions are same as Figs. 11 and 14 captions respectively.

aggregation (Oberdisse, 2006; Gao et al., 2011), while these effects are not central to the cylindrical morphology. This argument is experimentally proven by Do et al. (2012) and Liu et al. (2017). Further, Do et al. (2012) concluded the same trend as us.

We have also directly compared our model predictions with the results for the enhancement of the ionic conductivity of homogeneous polymers subjected to applied strain, from Kelly et al. (2016), Berg et al. (2018). As shown in Fig. 17 we observe a good match between the experimental data and our model for homogeneous materials. The qualitative match is nearly perfect and shows the linear enhancement of the ionic conductivity due to stretching as observed in the experiments (Kelly et al., 2016; Berg et al., 2018). We remark here that there is uncertainty in the estimation of certain material parameters. Most of our values are grounded in the literature or taken from the experimental papers. We have made reasonable choices of unavailable parameters such as λ_r and α_{el} to facilitate comparison with the experiments.

We also extracted the data of enhancement of ionic conductivity due to the addition of Al_2O_3 inclusions to the polymer matrix from Pitawala et al. (2007) and compared with our model predictions. As can be seen in Fig. 18, our model can well-predict the

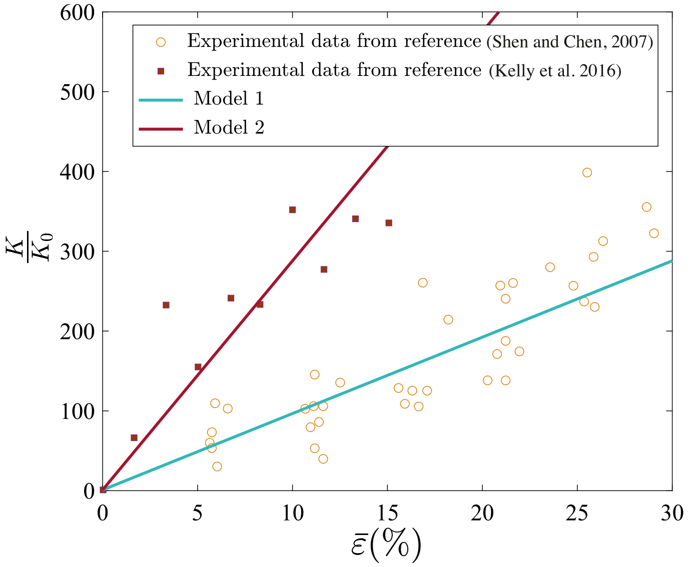

Fig. 17. Comparison of the normalized ionic conductivity with respect to the applied stretch between the constructed models and extracted experimental measurements from Berg et al. (2018), Kelly et al. (2016) respectively. The numerical values are $c_0 = 1500$ mole/m^3 (Grazioli et al., 2019), $\epsilon_r = 8$ (Bruce, 1997), $E_y = 0.03$ GPa (Maitra et al., 2007). To ensure quantitative agreement we fit the following: $\lambda_r = 4$ nm and $\alpha_{\mathrm{el}} = -10^{-15} \times [5, 15]$ J for the Model 1 and Model 2 respectively.

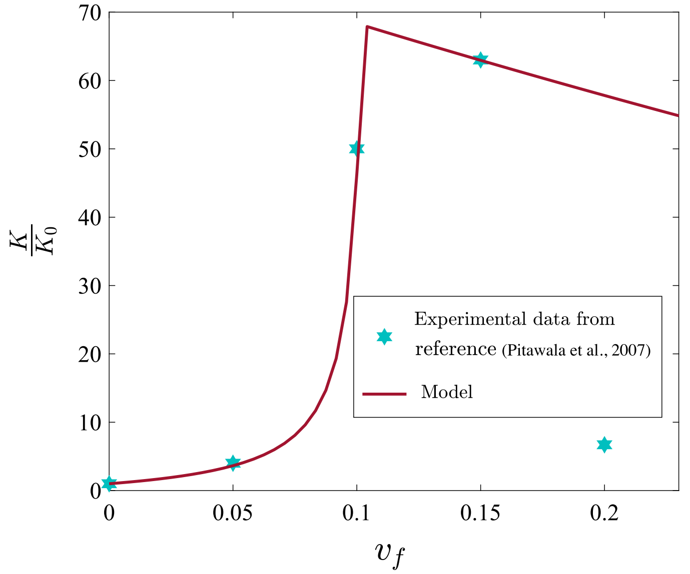

Fig. 18. Comparison of the normalized ionic conductivity with respect to the volume fraction of the inclusions between extracted experimental measurements (Pitawala et al., 2007) and analysis by our model. The numerical values are $c_0^{(1)} = 0$ mole/m^3, $c_0^{(2)} = c_0^{(3)} = 1500$ mole/m^3 (Grazioli et al., 2019), $\Delta\hat{\mu} = \hat{\mu}^{(3)} - \hat{\mu}^{(1)} = 1$ eV, $\hat{\mu}^{(2)} = \hat{\mu}^{(3)}$, $\lambda_r^{(1)} = \lambda_r^{(2)} = \lambda_r^{(3)} = 4$ nm, $\epsilon_r^{(1)} = 9$ (Rajab et al., 2008) and $\epsilon_r^{(2)} = \epsilon_r^{(3)} = 8$ (Bruce, 1997) and $\gamma_1 = \gamma_3$. To ensure quantitative agreement we fit the following: $\alpha = 0.57$ and $\gamma_2/\gamma_1 = 80$.

experimental measurements for smaller volume fractions. The trend and numerical disagreement at larger volume fractions is likely due to effects not considered in our homogenization process e.g. increased tortuosity in the transportation path of the ions (Shen and Chen, 2007), ion trapping and pairing and aggregation (Oberdisse, 2006; Gao et al., 2011).

6. Concluding remarks

We have presented a theory for the electro-chemo-mechanical behavior of soft deformable solid electrolytes. This general theory is easily adaptable to situations beyond what we have considered. The governing equations are highly coupled and nonlinear and rigorous homogenization results for heterogeneous electrolytes are thus difficult to obtain. Guided by the solutions to simple boundary value problems and the ensuing insights, we have outlined a simple homogenization strategy for obtaining the effective ionic conductivity of soft heterogeneous electrolytes. Using our approach, we can also easily establish Hashin–Shtrikman bounds.

Experimental observations show that the addition of active/passive fillers to the polymer matrix, results in the growth of an interphase region around filler which inherit high mobility (Siekierski et al., 2007; Johan et al., 2011; Sillamoni and Idiart, 2015). The extent of the interphase region is a function of the microstructure morphology, the materials involved and the fabrication method. The optimum size and volume fraction of fillers which results in higher ionic conductivity is obtained from a competition between the interphase extent, the domination of the interphase region in the polymer matrix and the amount of available ions in the system. While both active and passive fillers to some extent result in the improvement of the ionic conductivity, the active fillers are more effective. The size of the inclusions play a crucial role on the emergent ionic conductivity and the maximum value is obtained at the critical size of the inclusion introduced in the paper. Roughly speaking, larger inclusions have very low and even adverse impact in the ionic conductivity of the composite electrolytes. Insofar as deformation is concerned, stretching enhances the ionic conductivity of the composite polymer by increasing the number of available ions and enhancing the mobility of the polymer matrix.

The contradictory experimental results that exist in the literature regarding the effect of fillers may be explained by the insights provided by our model regarding the effect of microstructure length scale vis-a-vis system characteristics like the Debye length, among features (such as fabrication method) which are implicitly considered in our work in the sense of how they impact phenomenological features such as interphase extent etc.

We remark that recently several works have appeared that exploit molecular scale mechanisms to design electromechanical coupling in elastomers (Grasinger et al., 2021; Grasinger and Dayal, 2021; Cohen and deBotton, 2016; Grasinger and Dayal, 2020; Cohen et al., 2016). A similar study, in the context of non-equilibrium property like ionic conductivity, would be an interesting future endeavor.

CRediT authorship contribution statement

Kosar Mozaffari: Participated in development of the study and in writing the manuscript, Commented on the manuscript and gave approval for publication. **Liping Liu:** Participated in development of the study and in writing the manuscript, Commented on the manuscript and gave approval for publication. **Pradeep Sharma:** Participated in development of the study and in writing the manuscript, Commented on the manuscript and gave approval for publication.

Declaration of competing interest

The authors declare that they have no known competing financial interests or personal relationships that could have appeared to influence the work reported in this paper.

Acknowledgment

We gratefully acknowledge partial support from the M.D. Anderson Professorship.

Appendix A. Recovery of existing models for complex non-equilibrium processes

The formulation presented in Section 2 is versatile and can incorporate a variety of materials models in the literature. Below we present a few examples.

1. Biot's poroelasticity. A widely-used elastic-diffusion/permeation model in geophysics concerns the interaction of a porous solid and fluid where the kinematic variables include the deformation $\mathbf{y} : \Omega_R \to \mathbb{R}^3$ and fluid concentration $c : \Omega_R \to \mathbb{R}^+$. As a conservation law independent of energetics of the system, we introduce a primitive concept, the flux of fluid transport $\mathbf{J} : \Omega_R \to \mathbb{R}^3$, and enforce the conservation law (3) as a constraint:

$$\dot{c} + \mathrm{div}\mathbf{J} = 0 \quad \text{in } \Omega_R. \tag{98}$$

In the simplest scenario, we assume *isotropic* linearized elasticity and diffusion for which the free energy functional (5) and the dissipation-rate functional (16) are postulated as

$$\begin{aligned} &U_b[\mathbf{y}, c] = \int_{\Omega_R} \Psi(\nabla\mathbf{y}, c), \qquad \dot{D}[\mathbf{y}, \dot{\mathbf{y}}, c, \dot{c}, \mathbf{J}] = \int_{\Omega_R} \gamma|\mathbf{J}|^2, \\ &\Psi(\mathbf{F}, c) = \frac{1}{2}(\mathbf{F}-\mathbf{I})\cdot\mathbb{C}(\mathbf{F}-\mathbf{I}) + \alpha_{\mathrm{el}}(c-c_0)\mathrm{Tr}(\mathbf{F}-\mathbf{I}) + \frac{\beta}{2}(c-c_0)^2, \end{aligned} \tag{99}$$

respectively. Here, $\mathbb{C}$ is the fourth-order isotropic elasticity tensor with shear modulus G and Poisson's ratio ν, $\gamma > 0$ is now called the permeability coefficient, $\beta > 0$ is required by stability, and α_{el} is the coupling coefficients between strain and fluid concentration.

The rate of work done to the system is still identified as (4) at the absence of external body forces and sinks or sources. Upon repeating the calculations in Section 2.1 or directly from (11), we obtain[19]

$$\begin{aligned} \dot{D} = \dot{W} - \dot{U}_b = &\int_{\Omega_R} [(\mathrm{div}\mathbf{P}) \cdot \dot{\mathbf{y}} - \mathbf{J} \cdot \nabla \mu] \\ &+ \int_{\partial \Omega_R} \dot{\mathbf{y}} \cdot (\mathbf{t}^e - \mathbf{P}\mathbf{n}) - \int_{\Upsilon_D} (\mathbf{J} \cdot \mathbf{n})(\mu^e - \mu), \end{aligned} \tag{100}$$

where, from (8) and (99),

$$\mathbf{P} = \mathbb{C}(\mathbf{F} - \mathbf{I}) + \alpha_{\mathrm{el}}(c - c_0)\mathbf{I}, \qquad \mu = \alpha_{\mathrm{el}}\mathrm{Tr}(\mathbf{F} - \mathbf{I}) + \beta(c - c_0).$$

Consequently, by (17) and (18) the governing equations for the poroelasticity model can be written as follows:

$$\begin{cases} \mathrm{div}(\mathbb{C}\nabla\mathbf{u} + \alpha_{\mathrm{el}}(c - c_0)\mathbf{I}) = 0 & \text{in } \Omega_R, \\ \dot{c} = \mathrm{div}(\beta\gamma\nabla c + \gamma\alpha_{\mathrm{el}}\nabla(\nabla \cdot \mathbf{u})) & \text{in } \Omega_R, \end{cases}$$

which are equivalent to Eq. (81)–(82) in Detournay (1993) upon setting $c_0 \equiv 0$ and appropriate re-definition of material constants.

2. Nonlinear swelling models of fluid permeable elastomers. Elastomeric gels are permeable to fluids of small molecules. The gels swell or shrink upon absorption of fluids and fluids can be squeezed out of the gel. A continuum theory for fluid permeable elastomers has been established in Chester and Anand (2010). Their theory can be recovered from our formulation upon postulating the following kinematic constraint, free energy density function and dissipation potential:

$$\begin{aligned} &\text{kinematic constraint: } \lambda_s = (1 + \upsilon c)^{1/3}, \\ &U_b[\mathbf{y}, c] = \int_{\Omega_R} \Psi(\nabla\mathbf{y}, c), \qquad \dot{D}[\mathbf{y}, \dot{\mathbf{y}}, c, \dot{c}] = \int_{\Omega_R} \gamma|\mathbf{J}|^2 + \nabla\dot{\mathbf{y}} \cdot \mathbb{C}_{\mathrm{visc}}\nabla\dot{\mathbf{y}}, \\ &\Psi(\mathbf{F}, c) = \hat{\mu}c + \Psi_{\mathrm{mix}}(c) + \Psi_{\mathrm{mech}}(\frac{1}{\lambda_s}\mathbf{F}, c), \end{aligned} \tag{101}$$

where υ characterizes the volume occupied by fluid molecules, $\mathbb{C}_{\mathrm{visc}}$ reflects dissipation associated with strain rate, and Ψ_{mix} and Ψ_{mech} separate the contribution to the free energy from fluids and elastic deformation. For simplicity, we may neglect viscosity ($\mathbb{C}_{\mathrm{visc}} \equiv 0$) for slow processes. For a realistic description of elastomeric gels under large deformation, we may necessarily assume the mobility γ depend on deformation gradient and concentration and some general forms of Ψ_{mix} and Ψ_{mech}.

Appendix B. Elastically incompressible electro-elastic-diffusion model

For soft polymeric materials, it is common to assume elastic incompressibility since the bulk modulus is many orders of magnitude larger than the shear modulus. On the other hand, the permeation of charged ions (or uncharged molecules) induces significant volume change of the material. To model this phenomenon, we may enforce a kinematic constraint:

$$\Phi(\mathbf{F}, c) = \det\mathbf{F} - (1 + \nu(c - c_0)) = 0, \tag{102}$$

where ν can be interpreted as the volume of the mobile ions. The constraint (102) can be accounted for in our general formulation in Section 2.2 by the method of Lagrange multiplier. For instance, assume incompressible neo-Hookean elastic behaviors for the material. In account of the constraint (102), the free energy density of the body Ω_R can be written as

$$\Psi(\mathbf{F}, c) = \frac{1}{2}G(|\mathbf{F}|^2 - 3) + \frac{\beta}{2}(c - c_0)^2 + \hat{\mu}(c - c_0) - \Pi\Phi(\mathbf{F}, c), \tag{103}$$

where G is the shear modulus, and the direct coupling term $\alpha_{\mathrm{el}}(c - c_0)\mathrm{Tr}(\mathbf{F} - \mathbf{I})$ between c and $\mathbf{F}$ has to vanish because of elastic incompressibility. Upon repeating the argument in Section 2.2, we obtain the governing equations:

$$\begin{cases} \mathrm{div}(\mathbf{P} + \boldsymbol{\Sigma}_{\mathrm{MW}}) = 0 & \text{in } \Omega_R, \\ \dot{c} = \mathrm{div}[\gamma c\nabla(\mu + q\xi)] & \text{in } \Omega_R, \end{cases}$$

where

$$\mathbf{P} = G\mathbf{F} - J\Pi\mathbf{F}^{-T}, \qquad \mu = \hat{\mu} + \beta(c - c_0) + \Pi\nu.$$

---

[19] To relate with the conventional approach and notation in poroelasticity, say, Detournay (1993), we identify c as the fluid content ζ, $\mathbf{J}$ as the specific discharge vector $\mathbf{q}$, and μ as the pore pressure p. By some straightforward algebra, we can also identify the correspondence between material constants $(G, \nu, \alpha_{\mathrm{el}}, \beta)$ with the materials constants in Eqs. (54)–(57) in Detournay (1993). Further, one may assume the macroscopic Poisson ratio ν depends on the fluid content c so as to recover the exact Eq. (81)–(82) in Detournay (1993).

References

Ardebili, H., 2020. A perspective on the mechanics issues in soft solid electrolytes and the development of next-generation batteries. J. Appl. Mech. 87 (4).

Aurbach, D., Lu, Z., Schechter, A., Gofer, Y., Gizbar, H., Turgeman, R., Cohen, Y., Moshkovich, M., Levi, E., 2000. Prototype systems for rechargeable magnesium batteries. Nature 407 (6805), 724–727.

Bachman, J.C., Muy, S., Grimaud, A., Chang, H.-H., Pour, N., Lux, S.F., Paschos, O., Maglia, F., Lupart, S., Lamp, P., et al., 2016. Inorganic solid-state electrolytes for lithium batteries: mechanisms and properties governing ion conduction. Chem. Rev. 116 (1), 140–162.

Balaish, M., Kraytsberg, A., Ein-Eli, Y., 2014. A critical review on lithium–air battery electrolytes. Phys. Chem. Chem. Phys. 16 (7), 2801–2822.

Berg, S., Kelly, T., Porat, I., Moradi-Ghadi, B., Ardebili, H., 2018. Mechanical deformation effects on ion conduction in stretchable polymer electrolytes. Appl. Phys. Lett. 113 (8), 083903.

Bower, A.F., Guduru, P.R., Sethuraman, V.A., 2011. A finite strain model of stress, diffusion, plastic flow, and electrochemical reactions in a lithium-ion half-cell. J. Mech. Phys. Solids 59 (4), 804–828.

Bruce, P.G., 1997. Solid State Electrochemistry. vol. 5, Cambridge University Press.

Bruce, P.G., Freunberger, S.A., Hardwick, L.J., Tarascon, J.-M., 2012. Li–O 2 and Li–S batteries with high energy storage. Nature Mater. 11 (1), 19–29.

Chan, C.K., Peng, H., Liu, G., McIlwrath, K., Zhang, X.F., Huggins, R.A., Cui, Y., 2008. High-performance lithium battery anodes using silicon nanowires. Nature Nanotechnol. 3 (1), 31.

Chang, C., Li, X., Xu, Z., 2018. Microstructure-and concentration-dependence of lithium diffusion in the silicon anode: Kinetic Monte Carlo simulations and complex network analysis. Appl. Phys. Lett. 113 (12), 121904.

Chester, S.A., Anand, L., 2010. A coupled theory of fluid permeation and large deformations for elastomeric materials. J. Mech. Phys. Solids 58 (11), 1879–1906.

Cho, J.H., Xiao, X., Guo, K., Liu, Y., Gao, H., Sheldon, B.W., 2020. Stress evolution in lithium metal electrodes. Energy Storage Mater 24, 281–290.

Chon, M.J., Sethuraman, V.A., McCormick, A., Srinivasan, V., Guduru, P.R., 2011. Real-time measurement of stress and damage evolution during initial lithiation of crystalline silicon. Phys. Rev. Lett. 107 (4), 045503.

Chu, S., Majumdar, A., 2012. Opportunities and challenges for a sustainable energy future. Nature 488 (7411), 294–303.

Cohen, N., Dayal, K., deBotton, G., 2016. Electroelasticity of polymer networks. J. Mech. Phys. Solids 92, 105–126.

Cohen, N., deBotton, G., 2016. Electromechanical interplay in deformable dielectric elastomer networks. Phys. Rev. Lett. 116 (20), 208303.

Darbaniyan, F., Dayal, K., Liu, L., Sharma, P., 2019. Designing soft pyroelectric and electrocaloric materials using electrets. Soft Matter 15 (2), 262–277.

Darbaniyan, F., Yan, X., Sharma, P., 2020. An atomistic perspective on the effect of strain rate and lithium fraction on the mechanical behavior of silicon electrodes. J. Appl. Mech. 87 (3).

Detournay, E., 1993. Comprehensive rock engineering: Principles, practice and projects. Fund. Poroelasticity 2, 113–171.

Di Leo, C.V., Rejovitzky, E., Anand, L., 2014. A Cahn–Hilliard-type phase-field theory for species diffusion coupled with large elastic deformations: application to phase-separating Li-ion electrode materials. J. Mech. Phys. Solids 70, 1–29.

Do, N.S.T., Schaetzl, D.M., Dey, B., Seabaugh, A.C., Fullerton-Shirey, S.K., 2012. Influence of Fe2O3 nanofiller shape on the conductivity and thermal properties of solid polymer electrolytes: nanorods versus nanospheres. J. Phys. Chem. C 116 (40), 21216–21223.

Fan, L., Wei, S., Li, S., Li, Q., Lu, Y., 2018. Recent progress of the solid-state electrolytes for high-energy metal-based batteries. Adv. Energy Mater 8 (11), 1702657.

Fenton, D., 1973. Complexes of alkali metal ions with poly (ethylene oxide). Polymer 14, 589.

Fullerton-Shirey, S.K., Maranas, J.K., 2009. Effect of LiClO4 on the structure and mobility of PEO-based solid polymer electrolytes. Macromolecules 42 (6), 2142–2156.

Ganser, M., Hildebrand, F.E., Kamlah, M., McMeeking, R.M., 2019. A finite strain electro-chemo-mechanical theory for ion transport with application to binary solid electrolytes. J. Mech. Phys. Solids 125, 681–713.

Gao, F., Hong, W., 2016. Phase-field model for the two-phase lithiation of silicon. J. Mech. Phys. Solids 94, 18–32.

Gao, J., Qu, R., Tang, B., Wang, C., Ma, Q., Sun, C., 2011. Control of the aggregation behavior of silver nanoparticles in polyurethane matrix. J. Nanopart Res 13 (10), 5289.

Golodnitsky, D., Livshits, E., Peled, E., 2003. Highly conductive oriented PEO-based polymer electrolytes. In: Macromolecular Symposia. 203, (1), Wiley Online Library, pp. 27–46.

Golodnitsky, D., Peled, E., 2000. Stretching-induced conductivity enhancement of LiI(PEO)-polymer electrolyte. Electrochim. Acta 45 (8–9), 1431–1436.

Goodenough, J.B., Park, K.-S., 2013. The Li-ion rechargeable battery: a perspective. J. Am. Chem. Soc. 135 (4), 1167–1176.

Grasinger, M., Dayal, K., 2020. Statistical mechanical analysis of the electromechanical coupling in an electrically-responsive polymer chain. Soft Matter 16 (27), 6265–6284.

Grasinger, M., Dayal, K., 2021. Architected elastomer networks for optimal electromechanical response. J. Mech. Phys. Solids 146, 104171.

Grasinger, M., Mozaffari, K., Sharma, P., 2021. Flexoelectricity in soft elastomers and the molecular mechanisms underpinning the design and emergence of giant flexoelectricity. Proc. Natl. Acad. Sci. 118 (21).

Gray, F.M., Gray, F.M., 1991. Solid Polymer Electrolytes: Fundamentals and Technological Applications. VCH New York.

Grazioli, D., Verners, O., Zadin, V., Brandell, D., Simone, A., 2019. Electrochemical-mechanical modeling of solid polymer electrolytes: Impact of mechanical stresses on Li-ion battery performance. Electrochim. Acta 296, 1122–1141.

Guo, K., Kumar, R., Xiao, X., Sheldon, B.W., Gao, H., 2020. Failure progression in the solid electrolyte interphase (SEI) on silicon electrodes. Nano Energy 68, 104257.

Guo, K., Tamirisa, P.A., Sheldon, B.W., Xiao, X., Gao, H., 2018. Pop-up delamination of electrodes in solid-state batteries. J. Electrochem. Soc. 165 (3), A618.

Hashin, Z., Shtrikman, S., 1962a. On some variational principles in anisotropic and nonhomogeneous elasticity. J. Mech. Phys. Solids 10 (4), 335–342.

Hashin, Z., Shtrikman, S., 1962b. A variational approach to the theory of the effective magnetic permeability of multiphase materials. J. Appl. Phys. 33 (10), 3125–3131.

Hashin, Z., Shtrikman, S., 1963. A variational approach to the theory of the elastic behaviour of multiphase materials. J. Mech. Phys. Solids 11 (2), 127–140.

Hong, W., Zhao, X., Suo, Z., 2010. Large deformation and electrochemistry of polyelectrolyte gels. J. Mech. Phys. Solids 58 (4), 558–577.

Ito, Y., Nohira, T., 2000. Non-conventional electrolytes for electrochemical applications. Electrochim. Acta 45 (15–16), 2611–2622.

Johan, M.R., Shy, O.H., Ibrahim, S., Yassin, S.M.M., Hui, T.Y., 2011. Effects of Al2O3 nanofiller and EC plasticizer on the ionic conductivity enhancement of solid PEO–LiCF3SO3 solid polymer electrolyte. Solid State Ion. 196 (1), 41–47.

Jung, H.-G., Hassoun, J., Park, J.-B., Sun, Y.-K., Scrosati, B., 2012. An improved high-performance lithium–air battery. Nature Chem. 4 (7), 579.

Kasavajjula, U., Wang, C., Appleby, A.J., 2007. Nano-and bulk-silicon-based insertion anodes for lithium-ion secondary cells. J. Power Sources 163 (2), 1003–1039.

Kelly, T., Ghadi, B.M., Berg, S., Ardebili, H., 2016. In situ study of strain-dependent ion conductivity of stretchable polyethylene oxide electrolyte. Sci. Rep. 6 (1), 1–9.

Keplinger, C., Sun, J.-Y., Foo, C.C., Rothemund, P., Whitesides, G.M., Suo, Z., 2013. Stretchable, transparent, ionic conductors. Science 341 (6149), 984–987.

Kovetz, A., 2000. Electromagnetic Theory. vol. 975, Oxford University Press Oxford.

Lang, J., Ding, B., Zhu, T., Su, H., Luo, H., Qi, L., Liu, K., Wang, K., Hussain, N., Zhao, C., et al., 2016. Cycling of a lithium-ion battery with a silicon anode drives large mechanical actuation. Adv. Mater. 28 (46), 10236–10243.

Larche, F., Cahn, J., 1982. The effect of self-stress on diffusion in solids. Acta Metall. 30 (10), 1835–1845.

Lee, S.W., Lee, H.-W., Ryu, I., Nix, W.D., Gao, H., Cui, Y., 2015. Kinetics and fracture resistance of lithiated silicon nanostructure pairs controlled by their mechanical interaction. Nature Commun. 6 (1), 1–7.

Li, Q., Ardebili, H., 2014. Atomistic investigation of the nanoparticle size and shape effects on ionic conductivity of solid polymer electrolytes. Solid State Ion. 268, 156–161.

Li, Q., Chen, J., Fan, L., Kong, X., Lu, Y., 2016. Progress in electrolytes for rechargeable Li-based batteries and beyond. Green Energy Environ 1 (1), 18–42.

Li, Y., Cheng, X., Zhang, Y., Zhao, K., 2019. Recent advance in understanding the electro-chemo-mechanical behavior of lithium-ion batteries by electron microscopy. Materials Today Nano 7, 100040.

Li, Q., Wood, E., Ardebili, H., 2013. Elucidating the mechanisms of ion conductivity enhancement in polymer nanocomposite electrolytes for lithium ion batteries. Appl. Phys. Lett. 102 (24), 243903.

Liu, L., 2010. Hashin–shtrikman bounds and their attainability for multi-phase composites. Proc. R Soc A: Math, Phys Eng Sci 466 (2124), 3693–3713.

Liu, L., 2013. On energy formulations of electrostatics for continuum media. J. Mech. Phys. Solids 61 (4), 968–990.

Liu, W., Lee, S.W., Lin, D., Shi, F., Wang, S., Sendek, A.D., Cui, Y., 2017. Enhancing ionic conductivity in composite polymer electrolytes with well-aligned ceramic nanowires. Nat. Energy 2 (5), 1–7.

Liu, W., Liu, N., Sun, J., Hsu, P.-C., Li, Y., Lee, H.-W., Cui, Y., 2015. Ionic conductivity enhancement of polymer electrolytes with ceramic nanowire fillers. Nano Lett. 15 (4), 2740–2745.

Lukatskaya, M.R., Dunn, B., Gogotsi, Y., 2016. Multidimensional materials and device architectures for future hybrid energy storage. Nature Commun. 7 (1), 1–13.

MacGlashan, G.S., Andreev, Y.G., Bruce, P.G., 1999. Structure of the polymer electrolyte poly (ethylene oxide) 6: LiAsF 6. Nature 398 (6730), 792–794.

Maitra, M.G., Sinha, M., Mukhopadhyay, A.K., Middya, T.R., De, U., Tarafdar, S., 2007. Ion-conductivity and Young's modulus of the polymer electrolyte PEO–ammonium perchlorate. Solid State Ion. 178 (3–4), 167–171.

Manthiram, A., Fu, Y., Chung, S.-H., Zu, C., Su, Y.-S., 2014. Rechargeable lithium–sulfur batteries. Chem. Rev. 114 (23), 11751–11787.

Manthiram, A., Yu, X., 2015. Ambient temperature sodium–sulfur batteries. Small 11 (18), 2108–2114.

Manthiram, A., Yu, X., Wang, S., 2017. Lithium battery chemistries enabled by solid-state electrolytes. Nat. Rev Mater 2 (4), 1–16.

Marshall, J., Dayal, K., 2014. Atomistic-to-continuum multiscale modeling with long-range electrostatic interactions in ionic solids. J. Mech. Phys. Solids 62, 137–162.

Milton, G.W., Sawicki, A., 2003. Theory of composites. Cambridge monographs on applied and computational mathematics. Appl. Mech. Rev. 56 (2), B27–B28.

Minami, T., 2006. Solid State Ionics for Batteries. Springer Science & Business Media.

Narayan, S., Stewart, E.M., Anand, L., 2021. Coupled electro-chemo-elasticity: Application to modeling the actuation response of ionic polymer-metal composites. J. Mech. Phys. Solids 104394.

Oberdisse, J., 2006. Aggregation of colloidal nanoparticles in polymer matrices. Soft Matter 2 (1), 29–36.

Pitawala, H., Dissanayake, M., Seneviratne, V., 2007. Combined effect of Al2O3 nano-fillers and EC plasticizer on ionic conductivity enhancement in the solid polymer electrolyte (PEO) 9LiTf. Solid State Ion. 178 (13–14), 885–888.

Quartarone, E., Mustarelli, P., 2011. Electrolytes for solid-state lithium rechargeable batteries: recent advances and perspectives. Chem. Soc. Rev. 40 (5), 2525–2540.

Quartarone, E., Mustarelli, P., 2020. Emerging trends in the design of electrolytes for lithium and post-lithium batteries. J. Electrochem. Soc. 167 (5), 050508.

Rajab, K.Z., Naftaly, M., Linfield, E.H., Nino, J.C., Arenas, D., Tanner, D., Mittra, R., Lanagan, M., 2008. Broadband dielectric characterization of aluminum oxide (Al2O3). J. Microelectronics Electronic Packaging 5 (1), 2–7.

Rejovitzky, E., Di Leo, C.V., Anand, L., 2015. A theory and a simulation capability for the growth of a solid electrolyte interphase layer at an anode particle in a Li-ion battery. J. Mech. Phys. Solids 78, 210–230.

Roy, P., Srivastava, S.K., 2015. Nanostructured anode materials for lithium ion batteries. J. Mater. Chem. A 3 (6), 2454–2484.

Sethuraman, V.A., Chon, M.J., Shimshak, M., Srinivasan, V., Guduru, P.R., 2010. In situ measurements of stress evolution in silicon thin films during electrochemical lithiation and delithiation. J. Power Sources 195 (15), 5062–5066.

Shen, L., Chen, Z., 2007. Critical review of the impact of tortuosity on diffusion. Chem. Eng. Sci. 62 (14), 3748–3755.

Shen, X., Zhang, R., Chen, X., Cheng, X.-B., Li, X., Zhang, Q., 2020. The failure of solid electrolyte interphase on Li metal anode: structural uniformity or mechanical strength? Advanced Energy Mater 10 (10), 1903645.

Siekierski, M., Wieczorek, W., Nadara, K., 2007. Mesoscale models of conductivity in polymeric electrolytes—A comparative study. Electrochim. Acta 53 (4), 1556–1567.

Sillamoni, I.J.C., Idiart, M.I., 2015. A model problem concerning ionic transport in microstructured solid electrolytes. Contin. Mech. Thermodyn. 27 (6), 941–957.

Song, T., Xia, J., Lee, J.-H., Lee, D.H., Kwon, M.-S., Choi, J.-M., Wu, J., Doo, S.K., Chang, H., Park, W.I., et al., 2010. Arrays of sealed silicon nanotubes as anodes for lithium ion batteries. Nano Lett. 10 (5), 1710–1716.

Stephan, A.M., 2006. Review on gel polymer electrolytes for lithium batteries. Eur. Polym. J. 42 (1), 21–42.

Sun, J.-Y., Keplinger, C., Whitesides, G.M., Suo, Z., 2014. Ionic skin. Adv. Mater. 26 (45), 7608–7614.

Tan, S.-J., Zeng, X.-X., Ma, Q., Wu, X.-W., Guo, Y.-G., 2018. Recent advancements in polymer-based composite electrolytes for rechargeable lithium batteries. Electrochem. Energy Rev 1 (2), 113–138.

Tang, C., Hackenberg, K., Fu, Q., Ajayan, P.M., Ardebili, H., 2012. High ion conducting polymer nanocomposite electrolytes using hybrid nanofillers. Nano Lett. 12 (3), 1152–1156.

Tarascon, J., Armand, M., 2001. Determination of the chemical diffusion coefficient of lithium in LiFePO4. Nature 414, 359–367.

Vaalma, C., Buchholz, D., Weil, M., Passerini, S., 2018. A cost and resource analysis of sodium-ion batteries. Nature Rev. Mater 3 (4), 1–11.

Wang, X., Hong, W., 2011. Theory of ionic polymer conductor network composite. Appl. Phys. Lett. 98 (8), 081910.

Wang, Y.-J., Pan, Y., Kim, D., 2006. Conductivity studies on ceramic Li1. 3Al0. 3Ti1. 7 (PO4) 3-filled PEO-based solid composite polymer electrolytes. J. Power Sources 159 (1), 690–701.

Wang, Y., Richards, W.D., Ong, S.P., Miara, L.J., Kim, J.C., Mo, Y., Ceder, G., 2015. Design principles for solid-state lithium superionic conductors. Nature Mater. 14 (10), 1026–1031.

Wang, P., Zakeeruddin, S.M., Exnar, I., Grätzel, M., 2002. High efficiency dye-sensitized nanocrystalline solar cells based on ionic liquid polymer gel electrolyte. Chem. Commun (24), 2972–2973.

Watanabe, M., Kanba, M., Matsuda, H., Tsunemi, K., Mizoguchi, K., Tsuchida, E., Shinohara, I., 1981. High lithium ionic conductivity of polymeric solid electrolytes. Die Makromolekulare Chemie, Rapid Commun 2 (12), 741–744.

Weston, J., Steele, B., 1982. Effects of inert fillers on the mechanical and electrochemical properties of lithium salt-poly (ethylene oxide) polymer electrolytes. Solid State Ion. 7 (1), 75–79.

Williard, N., He, W., Hendricks, C., Pecht, M., 2013. Lessons learned from the 787 Dreamliner issue on lithium-ion battery reliability. Energies 6 (9), 4682–4695.

Winter, M., Besenhard, J.O., 1999. Electrochemical lithiation of tin and tin-based intermetallics and composites. Electrochim. Acta 45 (1–2), 31–50.

Wypych, G., 2012. 2 - material composition, structure and morphological features. In: Wypych, G. (Ed.), Atlas of Material Damage. Elsevier, pp. 7–52.

Xiao, Y., Bhattacharya, K., 2008. A continuum theory of deformable, semiconducting ferroelectrics. Arch. Ration. Mech. Anal. 189 (1), 59–95.

Xiao, X., Zhou, W., Kim, Y., Ryu, I., Gu, M., Wang, C., Liu, G., Liu, Z., Gao, H., 2015. Regulated breathing effect of silicon negative electrode for dramatically enhanced performance of Li-ion battery. Adv. Funct. Mater. 25 (9), 1426–1433.

Xu, C., Mudunuru, M.K., Nakshatrala, K., 2016. Material degradation due to moisture and temperature. Part 1: Mathematical model, analysis, and analytical solutions. Contin. Mech. Thermodyn. 28 (6), 1847–1885.

Xu, S., Zhang, Y., Cho, J., Lee, J., Huang, X., Jia, L., Fan, J.A., Su, Y., Su, J., Zhang, H., et al., 2013. Stretchable batteries with self-similar serpentine interconnects and integrated wireless recharging systems. Nature Commun. 4 (1), 1–8.

Yan, X., Gouissem, A., Guduru, P.R., Sharma, P., 2017. Elucidating the atomistic mechanisms underpinning plasticity in Li-Si nanostructures. Phys. Rev. Mater 1 (5), 055401.

Yan, X., Gouissem, A., Sharma, P., 2015. Atomistic insights into Li-ion diffusion in amorphous silicon. Mech. Mater. 91, 306–312.

Yang, C., Fu, K., Zhang, Y., Hitz, E., Hu, L., 2017. Protected lithium-metal anodes in batteries: From liquid to solid. Adv. Mater. 29 (36), 1701169.

Yang, C., Suo, Z., 2018. Hydrogel ionotronics. Nat Rev. Mater 3 (6), 125.

Zhang, H., Dehghany, M., Hu, Y., 2020a. Kinetics of polyelectrolyte gels. J. Appl. Mech. 87 (6).

Zhang, Y., Huang, Y., Rogers, J.A., 2015. Mechanics of stretchable batteries and supercapacitors. Curr. Opin. Solid State Mater. Sci. 19 (3), 190–199.

Zhang, S., Li, Z., Guo, Y., Cai, L., Manikandan, P., Zhao, K., Li, Y., Pol, V.G., 2020b. Room-temperature, high-voltage solid-state lithium battery with composite solid polymer electrolyte with in-situ thermal safety study. Chem. Eng. J. 400, 125996.

Zhang, J., Yao, X., Misra, R.K., Cai, Q., Zhao, Y., 2020c. Progress in electrolytes for beyond-lithium-ion batteries. J. Mater. Sci Technol.

Zhao, K., Pharr, M., Cai, S., Vlassak, J.J., Suo, Z., 2011. Large plastic deformation in high-capacity lithium-ion batteries caused by charge and discharge. J. Am. Ceram. Soc. 94, s226–s235.

Zhao, K., Pharr, M., Vlassak, J.J., Suo, Z., 2010. Fracture of electrodes in lithium-ion batteries caused by fast charging. J. Appl. Phys. 108 (7), 073517.

Zhao, Q., Stalin, S., Zhao, C.-Z., Archer, L.A., 2020. Designing solid-state electrolytes for safe, energy-dense batteries. Nature Rev. Mater 1–24.

Zheng, Q., Wei, G.-W., 2011. Poisson–boltzmann–nernst–planck model. J. Chem. Phys. 134 (19), 194101.

Zito, R., Ardebili, H., 2019. Energy Storage: A New Approach. Wiley-Scrivener; 2 edition.

Zou, Z., Li, Y., Lu, Z., Wang, D., Cui, Y., Guo, B., Li, Y., Liang, X., Feng, J., Li, H., et al., 2020. Mobile ions in composite solids. Chem. Rev..